J. Fluid Mech. (1971), *vol.* 50, *part* 4, *pp.* 705–740
Printed in Great Britain

A new technique for treating multiparticle slow viscous flow: axisymmetric flow past spheres and spheroids†

By MICHAEL J. GLUCKMAN, ROBERT PFEFFER AND SHELDON WEINBAUM
The City College of The City University of New York

(Received 21 October 1970)

This paper is the first in a series of investigations having the overall objective of developing a new technique for treating the slow viscous motion past finite assemblages of particles of arbitrary shape. The new method, termed the multipole representation technique, is based on the theory that any object conforming to a natural co-ordinate system in a particle assemblage can be approximated by a truncated series of multi-lobular disturbances in which the accuracy of the representation is systematically improved by the addition of higher order multipoles. The essential elements of this theory are illustrated by examining the flows past finite line arrays of axisymmetric bodies such as spheres and spheroids which conform to special natural co-ordinate systems. It is demonstrated that this new procedure converges more rapidly and is simpler to use than the method of reflexions and represents the desired boundaries more precisely than the point-force approximation even when the objects are touching one another. Comparison of these solutions with the exact solutions of Stimson & Jeffery (1926) for the two sphere problem demonstrates the rapidity of convergence of this multipole procedure even when the spheres are touching. Drag results are also presented for flows past chains containing up to 101 spheres as well as for chains containing up to 15 prolate or oblate spheroids. The potential value of the technique is suggested by the rapidity with which the drag calculations were made, the 101 sphere problem requiring about 10 seconds on an IBM 360–65 computer to determine both the fluid flow and the drag coefficient.

1. Introduction

The slow motion of an incompressible viscous fluid relative to assemblages of submerged particles has long been of interest in the areas of sedimentation, flow through packed beds, the study of suspension viscosities, and other applications of two-phase flow. A review of the pertinent literature by Happel & Brenner (1965) indicates that two approaches – the method of reflexions and the point-force approximation – have been used extensively for treating multiparticle slow-flow problems. The method of reflexions, developed by Smoluchowski (1911, 1912) and used by Burgers (1940), Kynch (1959) and Happel & Brenner

† This paper was presented at the International Symposium on Two-Phase Systems, 29 August–2 September 1971, Technion City, Haifa, Israel.

(1965), is an iterative approximation technique. For the first reflexion, perturbations resulting from the velocity field due to one particle being reflected from the boundary of a second particle are used to correct the zeroth-order velocity field of the second particle calculated in the absence of the first particle. The nth-order reflexion is then the correction required to satisfy the no-slip boundary conditions at the surface of each object caused by the disturbance field of the $(n-1)$th reflexion of all other particles. This technique allows multiple particle interaction problems to be handled and has been shown to converge to the exact solution for the two sphere problem. The convergence characteristics are strongly dependent on the ratio of sphere spacing $2d$ to sphere diameter $2a$. When this ratio d/a is large (i.e. dilute system) a single reflexion describes the particle interactions adequately. For concentrated systems $(d/a \rightarrow 1)$ higher order interaction effects become significant and the leading term in the iterative series solution becomes a poor description of particle interaction effects and generates a series with very slow convergence characteristics.

The point-force approximation technique developed by Burgers (1938, 1941, 1942), and used by McNown & Lin (1952), Tchen (1954), Broersma (1960) and Tam (1969), requires that the disturbance produced by a submerged object be replaced by one or more point forces located at the foci of the object. This technique approximates the exact viscous no-slip boundary condition by requiring that the velocity over the surface of the sphere vanishes in some average sense. This approximate technique has also been used in conjunction with the method of reflexions to describe multiple particle interaction problems by Burgers (1941, 1942) and Kynch (1959). Since point forces radiate with equal intensity in all directions the angular dependence of disturbances on the boundaries of one spherical object in the presence of others cannot be taken into account. This angular dependence grows in importance as the angle subtended by the test sphere relative to the origins of the other spheres increases. Therefore, the accuracy of the point-force representation quickly diminishes as the spheres approach one another.

The techniques described above must in general be used when more than two objects are present except for the special case of the flow relative to an infinite chain of equally spaced spheres and spheriods along their line of centres. Because of the perfect periodicity existing in such an infinite chain this latter problem can be viewed as the flow past a single sphere or spheriod in a cell with periodic boundary conditions, e.g. Wang & Skalak (1969) and Chen & Skalak (1970). The numerous two sphere problems treated in the literature form an important class of exact solutions that provide valuable insight into the convergence characteristics of the method of reflexions and the accuracy of the point-force approximation. These exact solutions all depend on mapping the solution for a single sphere into spherical bipolar co-ordinates. This technique was first used by Stimson & Jeffery (1926), for two spheres translating along their line of centres, and was extended to the asymmetric case by Dean & O'Neill (1963). Further extensions of this problem have been reported by Goldman, Cox & Brenner (1966), slow motion of two identical arbitrarily oriented spheres, and by Davis (1969), translation and rotation of two unequal spheres.

The object of the present study is to develop a new technique for handling concentrated axisymmetric systems of particles conforming to natural co-ordinate systems which is capable of satisfying the no-slip boundary conditions more accurately than the point-force approximation technique and which also converges more rapidly than the method of reflexions. The new method is based on the concept that the disturbance due to each submerged object can be represented by an infinite series of multipoles placed at the centre of the object, where each multipole series has a different origin. The strength of each multipole is determined so as to satisfy the no-slip boundary conditions along the surface of all interacting particles simultaneously. To satisfy the boundary conditions exactly along a finite surface, multipoles of all orders must be retained in the same sense that a complete Fourier series is required to represent any well-behaved function over a finite interval. However, since each multipole used to represent a submerged object allows the exact no-slip boundary conditions to be satisfied at a point on the generating arc of that object, solutions of any order of accuracy can be obtained depending on the order of the multipoles retained in the solution. The technique is, therefore, one of truncation rather than an iterative procedure as in the method of reflexions. Furthermore, since all particles are treated simultaneously to the same order, the effect of other particles is considered even in the lowest order truncation. It will be shown that the lowest order truncation solution for the drag on each particle using the new technique is considerably more accurate than the first reflexion solution in the method of reflexions when the particles are close together and as good a solution as the point-force approximation when the particles are far apart. This improvement in accuracy over the method of reflexions increases as one goes to corresponding higher order corrections in each method.

The multipole representation technique can be used to describe the motion past any number of spherical objects by placing a multipole series at the focal point of each sphere. This reasoning is easily extended to oblate and prolate spheroids. The characteristic length between foci is then used to stretch or compress the lobes of each multipole originating from the geometrical centre of each spheroid. In principle, an arbitrary axisymmetric object can be represented by a continuous distribution of spheroidal co-ordinate multipoles of vanishing aspect ratio. From a practical point of view a good approximation to flow past complex shapes can be obtained using other objects, e.g. a long cylinder is well approximated by a string of prolate spheroids placed end to end. The present paper is restricted to the axisymmetric flow past spheres and spheroids in order to demonstrate the simplicity and utility of the multipole approach. A second paper treating arbitrary axisymmetric flow configurations is to appear separately. The technique is also currently being extended to non-axisymmetric problems.

In §2 the problem of flow past multiple spheres utilizing the multipole technique is formulated. Solutions for flow past two spheres are compared with the exact results of Stimson & Jeffery (1926) in §3 and solutions to flow past any finite number of equally spaced spheres are discussed in §4. Section 5 contains the formulation of the problem of flow past a number of submerged bifocal

objects in terms of multipoles. Results for multiple prolate and oblate spheroids are presented in §§6 and 7 respectively.

2. Formulation for multiple spheres

In this section, a general description and discussion of the multipole representation technique will be presented and applied to a general solution for slow viscous incompressible flow past a finite chain of equally spaced spheres.

By omitting the inertial terms, $\rho\mathbf{v}.\nabla\mathbf{v}$, the steady-state Navier–Stokes equations reduce to the well-known creeping motion or Stokes equations, i.e.

$$\nabla^2\mathbf{v} = (1/\mu)\nabla p. \tag{2.1}$$

To obtain an equation in a single dependent variable one introduces the stream function, defined in spherical co-ordinates as

$$V_r = -\frac{1}{r^2\sin\theta}\frac{\partial\psi}{\partial\theta}, \quad V_\theta = \frac{1}{r\sin\theta}\frac{\partial\psi}{\partial r}, \tag{2.2}$$

and takes the curl of (2.1) which results in the GASP equation

$$\nabla^2(\nabla^2\psi) = 0, \tag{2.3}$$

where ∇^2 is the slow motion Stokesian operator

$$\nabla^2 = \frac{\partial^2}{\partial r^2} + \frac{(1-\zeta^2)}{r^2}\frac{\partial^2}{\partial\zeta^2}$$

and

$$\zeta = \cos\theta.$$

The stream function ψ is related to the vorticity ω as follows:

$$\nabla^2\psi = 2\omega.$$

The general solution to (2.3), presented by Sampson (1891), Savic (1953) and Haberman & Sayre (1958), is based on the linearity of (2.3) and contains two basic summations

$$\psi = \psi_1 + \psi_2,$$

where ψ_1 contains the irrotational solutions $\nabla^2\psi_1 = 0$ and ψ_2 contains the rotational solutions $\nabla^2\psi_2 = 2\omega$;

$$\psi = \sum_{n=0}^{\infty}[A_n r^n + B_n r^{-n+1} + C_n r^{n+2} + D_n r^{-n+3}]I_n(\zeta) + \sum_{n=2}^{\infty}[A'_n r^n + B'_n r^{-n+1} + C'_n r^{n+2} + D'_n r^{-n+3}]H_n(\zeta), \tag{2.4}$$

where the terms $A_n r^n$, $B_n r^{-n+1}$, $A'_n r^n$ and $B'_n r^{-n+1}$ belong to ψ_1 and the terms $C_n r^{n+2}$, $D_n r^{-n+3}$, $C'_n r^{n+2}$ and $D'_n r^{-n+3}$ belong to ψ_2. Here $I_n(\zeta)$ and $H_n(\zeta)$ are Gegenbauer functions of the first and second kind respectively, related to Legendre functions as follows:

$$I_n(\zeta) = [P_{n-2}(\zeta) - P_n(\zeta)]/(2n-1) \quad \text{for} \quad n \geqslant 2,$$
$$H_n(\zeta) = [Q_{n-2}(\zeta) - Q_n(\zeta)]/(2n-1) \quad \text{for} \quad n \geqslant 2,$$

where $I_0(\zeta) = 1$, $I_1(\zeta) = -\zeta$, $H_0(\zeta) = -\zeta$, $H_1(\zeta) = -1$.

The condition of uniform flow at infinity in the direction of the negative x axis requires that

$$\psi \to \tfrac{1}{2}Ur^2\sin^2\theta \quad \text{as} \quad r\to\infty. \tag{2.5}$$

This condition plus the fact that the functions of the second kind ($H_n(\zeta)$) become infinite along the axis $\zeta = \pm 1$ results in the following evaluation of some of the constants in (2.4):

$$\left.\begin{aligned} &C_n = A'_n = B'_n = C'_n = D'_n = 0 \quad \text{for all } n,\\ &A_2 = U, \quad A_n = 0 \quad \text{for} \quad 3 \leqslant n < \infty. \end{aligned}\right\} \tag{2.6}$$

Application of (2.5) and (2.6) to (2.4) results in the following general form for the stream function in spherical co-ordinates:

$$\psi = \tfrac{1}{2}Ur^2\sin^2\theta + \sum_{n=2}^{\infty}[B_n r^{-n+1} + D_n r^{-n+3}]\, I_n(\zeta). \tag{2.7}$$

Sampson has shown that for flow past a single perfect sphere

$$B_n = D_n = 0 \quad \text{for} \quad n > 2;$$

(2.7) therefore reduces to the well-known single sphere result

$$\psi = \tfrac{1}{2}Ur^2\sin^2\theta + \tfrac{1}{2}\sin^2\theta\,[B_2/r + D_2 r].$$

Finally, B_2 and D_2 are determined by applying the no-slip boundary conditions to equations (2.2) evaluated at $r = a$.

The force exerted by the fluid on a spherical boundary r = constant is shown in Happel & Brenner (1965) to be

$$F = \mu\pi\int_0^{\pi} r^3\sin^3\theta\,\frac{\partial}{\partial r}\left(\frac{\nabla^2\psi}{r^2\sin^2\theta}\right) r\,d\theta.$$

Performing this integration on (2.7) and making use of the orthogonality of the Gegenbauer functions $I_n(\zeta)$, i.e.

$$\int_{-1}^{+1}\frac{I_m(\zeta)\,I_n(\zeta)}{1-\zeta^2}\,d\zeta = \begin{cases} 0 & \text{for} \quad m \neq n \\ 2/[n(n-1)\,(2n-1)] & \text{for} \quad m = n, \end{cases}$$

results in

$$F = 4\pi\mu D_2, \tag{2.8}$$

i.e. the drag on a single sphere is represented by the leading term in the infinite series solution for the rotational part of the flow. Equation (2.8) is an analogous result to that found by Wang & Skalak (1969) and Chen & Skalak (1970).

It is possible to extend Sampson's results for flow past a single sphere to the case of flow past any finite number of equally spaced spheres along their line of centres. The geometry of the system being considered is shown in figure 1. From the linearity of the governing equation of motion (2.3) it is possible to write the solution for the stream function for flow past N spheres as follows

$$\psi = \sum_{j=-\frac{1}{2}(N-1)}^{\frac{1}{2}(N-1)}\psi_j \quad \text{for} \quad N \text{ odd}, \tag{2.9a}$$

where the origin is taken on the centre sphere for convenience. For N even the origin is taken on the sphere closest to the centre of the chain, i.e.

$$\psi = \sum_{j=-\frac{1}{2}(N-2)}^{\frac{1}{2}N}\psi_j, \tag{2.9b}$$

where ψ_j is represented by (2.7), i.e.

$$\psi_j = \tfrac{1}{2}Ur_0^2 \sin^2\theta_0 + \sum_{n=2}^{\infty} [B_{nj} r_j^{-n+1} + D_{nj} r_j^{-n+3}] I_n(\zeta_j). \tag{2.10}$$

Here r_j and ζ_j are measured from the origin of each sphere considered separately. Combining (2.9) and (2.10) yields the following solution for the stream function for flow past N spheres

$$\psi = \tfrac{1}{2}Ur_0^2 \sin^2\theta_0 + \sum_{j=-\frac{1}{2}(N-1)}^{\frac{1}{2}(N-1)} \sum_{n=2}^{\infty} [B_{nj} r_j^{-n+1} + D_{nj} r_j^{-n+3}] I_n(\zeta_j). \tag{2.11}$$

In order to apply (2.11), the r_j and ζ_j terms must be written in terms of a single co-ordinate system, i.e.

$$r_j = [(x-2jd)^2 + y^2]^{\frac{1}{2}}$$

$$\zeta_j = (x-2jd)/r_j \quad -\tfrac{1}{2}(N-1) \leqslant j \leqslant \tfrac{1}{2}(N-1).$$

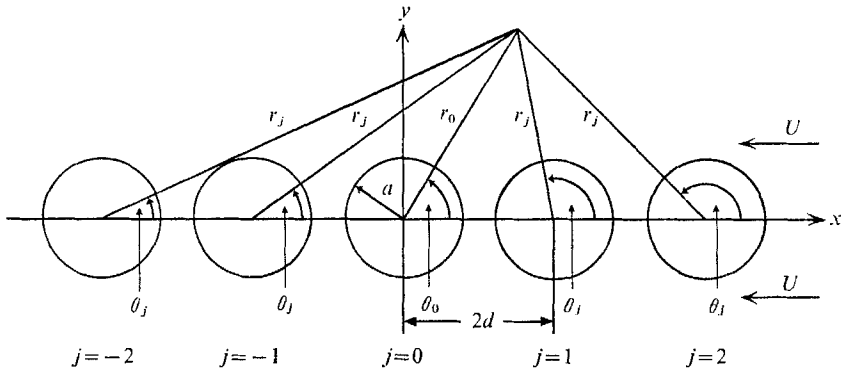

FIGURE 1. Geometry of the multiple sphere system.

Examination of the complete expression for the stream function (2.11) indicates that a double series expansion which is infinite in one dimension and can be large in the other dimension is required to represent the exact solution. The basic problem is to determine the constants in this two-dimensional series expansion so as to satisfy the no-slip viscous boundary conditions along the surfaces of all spheres considered simultaneously. A better insight into the flow representation of (2.11) can be had by examining the Gegenbauer functions of the first kind, i.e. $I_n(\zeta)$. Figure 2 demonstrates the form taken by $I_2(\cos\theta)$ to $I_5(\cos\theta)$. It can be seen from this figure that Gegenbauer functions of the first kind represent, conceptually, disturbances emanating from a single focal point. These disturbances are symmetrical about both axes and increase in complexity as the order of the Gegenbauer function increases. In general $I_n(\zeta_j)$ represents a disturbance which will have $2n-2$ lobes distributed symmetrically about the x axis. The term multipole has been coined to describe a single term in the inner series in (2.11). Thus each multipole has associated with it two constants B_{nj} and D_{nj} which are related to the intensity of the multipoles. These multipoles are somewhat akin to the Burgers point forces in that they represent disturbances radiating from a single focal point. They differ from point forces in that their intensity varies as a function of the polar angle θ_j.

Further examination of these multipoles in the context in which they appear in (2.11) leads to certain rather interesting conclusions. Each compound term or multipole in the inner series expansion for the solution for the stream function contains two constants operating on $I_n(\zeta_j)$. Now, for flow past spherical objects the no-slip boundary conditions on the surface of each object result in two

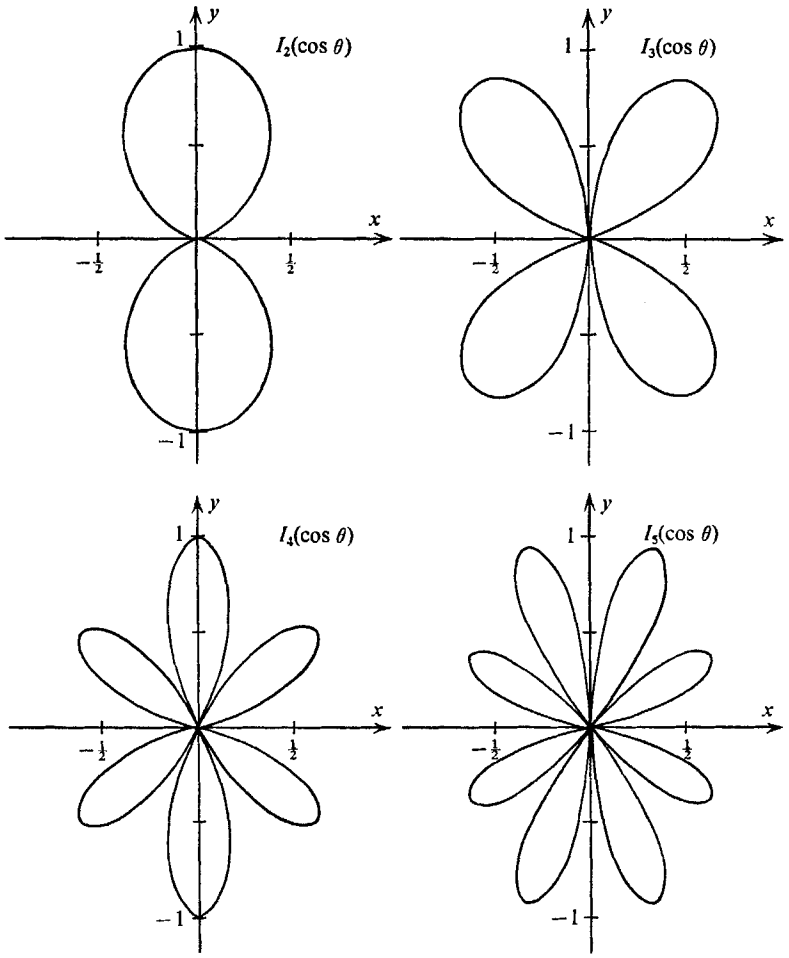

FIGURE 2. Graphical representations of Gegenbauer functions of the first kind.

equations for each discrete point on the semicircular arc of radius a that revolves about the x axis to form the sphere, i.e. at $r_j = a$ and $\theta_j = \theta_j$

$$\left.\begin{aligned} V_{rj} = 0 &= \partial\psi/\partial\theta_j, \\ V_{\theta j} = 0 &= \partial\psi/\partial r_j. \end{aligned}\right\} \tag{2.12}$$

The two arbitrary constants in each multipole thus provide the freedom to satisfy the boundary conditions (2.12) at one point along the generating arc of each sphere. If the boundary conditions are to be satisfied over the entire surface of each sphere (i.e. at an infinite number of points on the generating arc) an

infinite number of terms of multipoles would be required to represent the disturbance due to each submerged sphere.

The question of greatest practical importance is how many multipoles are required to represent each sphere in the chain to produce a result having the desired accuracy. The answer to this question is complex and will be the object of careful examination in subsequent sections where detailed comparisons with the known exact solution for two spheres are presented. One anticipates that the constants in each multipole will be a function of the dimensionless spacing d/a and that in the limit $d/a \to \infty$ all the higher order coefficients should become vanishingly small. This must occur if the multipole representation (2.11) is to reduce to the exact solution for a single sphere. The principle of series truncation described above has been employed for problems involving flows relative to single objects, i.e. O'Brien (1968), as well as flows relative to infinite chains of objects, where the boundary-value problem is that of a single periodic cell, i.e. Wang & Skalak (1969) and Chen & Skalak (1970). It has not, however, been investigated as a rational numerical procedure for problems involving flow relative to finite chains of objects.

Returning to the equation for the stream function (2.11) and using the boundary conditions (2.12) we shall now present in general form the solution to the problem of axisymmetric flow past an arbitrary number of equally spaced spherical objects. If a system of N spheres is spaced evenly along the x axis as depicted in figure 1 and the boundary conditions are satisfied at M points along the generating arc of each of the N spheres, then a set of $2 \times N \times M$ homogeneous simultaneous linear algebraic equations results for the $2 \times N \times M$ unknown constants B_{nj} and D_{nj}. The general solution for all the required constants in (2.11) can be represented as follows. Using (2.2), (2.11), (2.12) and the differential form for $I_n(\zeta)$, i.e.

$$d(I_n(\zeta))/d\zeta = -P_{n-1}(\zeta),$$

it can be shown that

$$\left.\begin{aligned} V_{rjm} &= A'_{jm} + \sum_{q=1}^{N} \sum_{n=2}^{M+1} [B'_{nqm} B_{nq} + D'_{nqm} D_{nq}] = 0, \\ V_{0jm} &= A''_{jm} + \sum_{q=1}^{N} \sum_{n=2}^{M+1} [B''_{nqm} B_{nq} + D''_{nqm} D_{nq}] = 0, \end{aligned}\right\} \tag{2.13a}$$

where, for $1 \leqslant m \leqslant N$,

$$\left.\begin{aligned} A'_{jm} &= -U \cos\theta_{jm}, \\ B'_{nqm} &= \frac{1}{r_{jm}^2 \sin\theta_{jm}} \left[(n-1) r_{qm}^{-n} \frac{\partial r_{qm}}{\partial \theta_{jm}} I_n(\zeta_{qm}) + r_{qm}^{-n+1} P_{n-1}(\zeta_{qm}) \frac{\partial \zeta_{qm}}{\partial \theta_{jm}} \right], \\ D'_{nqm} &= \frac{1}{r_{jm}^2 \sin\theta_{jm}} \left[(n-3) r_{qm}^{-n+2} \frac{\partial r_{qm}}{\partial \theta_{jm}} I_n(\zeta_{qm}) + r_{qm}^{-n+3} P_{n-1}(\zeta_{qm}) \frac{\partial \zeta_{qm}}{\partial \theta_{jm}} \right], \\ A''_{jm} &= U \sin\theta_{jm}, \\ B''_{nqm} &= \frac{1}{r_{jm} \sin\theta_{jm}} \left[(-n+1) r_{qm}^{-n} \frac{\partial r_{qm}}{\partial r_{jm}} I_n(\zeta_{qm}) - r_{qm}^{-n+1} P_{n-1}(\zeta_{qm}) \frac{\partial \zeta_{qm}}{\partial r_{jm}} \right], \\ D''_{nqm} &= \frac{1}{r_{jm} \sin\theta_{jm}} \left[(-n+3) r_{qm}^{-n+2} \frac{\partial r_{qm}}{\partial r_{jm}} I_n(\zeta_{qm}) - r_{qm}^{-n+3} P_{n-1}(\zeta_{qm}) \frac{\partial \zeta_{qm}}{\partial r_{jm}} \right]. \end{aligned}\right\} \tag{2.13b}$$

Equation (2.13), when written in matrix form, becomes

$$\begin{bmatrix} B'_{2,1,1} & D'_{2,1,1} & B'_{3,1,1} & D'_{3,1,1} & \dots B'_{M+1,N,1} & D'_{M+1,N,1} \\ B'_{2,1,2} & D'_{2,1,2} & B'_{3,1,2} & D'_{3,1,2} & \dots B'_{M+1,N,2} & D'_{M+1,N,2} \\ \cdot & \cdot & \cdot & \cdot & \cdot & \cdot \\ \cdot & \cdot & \cdot & \cdot & \cdot & \cdot \\ \cdot & \cdot & \cdot & \cdot & \cdot & \cdot \\ B'_{2,1,M} & D'_{2,1,M} & B'_{3,1,M} & D'_{3,1,M} & \dots B'_{M+1,N,M} & D'_{M+1,N,M} \\ B''_{2,1,1} & D''_{2,1,1} & B''_{3,1,1} & D''_{3,1,1} & \dots B''_{M+1,N,1} & D''_{M+1,N,1} \\ B''_{2,1,2} & D''_{2,1,2} & B''_{3,1,2} & D''_{3,1,2} & \dots B''_{M+1,N,2} & D''_{M+1,N,2} \\ \cdot & \cdot & \cdot & \cdot & \cdot & \cdot \\ \cdot & \cdot & \cdot & \cdot & \cdot & \cdot \\ \cdot & \cdot & \cdot & \cdot & \cdot & \cdot \\ B''_{2,1,M} & D''_{2,1,M} & B''_{3,1,M} & D''_{3,1,M} & \dots B''_{M+1,N,M} & D''_{M+1,N,M} \end{bmatrix} \begin{bmatrix} B_{2,1} \\ D_{2,1} \\ \cdot \\ \cdot \\ \cdot \\ D_{M+1,\frac{1}{2}(N-1)} \\ B_{2,\frac{1}{2}(N+1)} \\ D_{2,\frac{1}{2}(N+1)} \\ \cdot \\ \cdot \\ \cdot \\ D_{M+1,N} \end{bmatrix} = \begin{bmatrix} -A'_{1,1} \\ -A'_{1,2} \\ \cdot \\ \cdot \\ \cdot \\ -A'_{N,M} \\ -A''_{1,1} \\ -A''_{1,2} \\ \cdot \\ \cdot \\ \cdot \\ -A''_{N,M} \end{bmatrix}. \tag{2.14}$$

This linear set of simultaneous algebraic equations can be solved by any of the standard matrix reduction techniques (such as the Crout method) to yield the B_{nj} and D_{nj} constants required in equation (2.11) for the stream function.

The drag force exerted by the fluid on each sphere in the array can be determined from

$$F_j = \mu\pi \int_0^\pi r_j^3 \sin^3\theta_j \frac{\partial}{\partial r_j}\left[\frac{\nabla^2\psi}{r_j^2 \sin^2\theta_j}\right] r_j \, d\theta_j. \tag{2.15}$$

Performing the above integration and using the orthogonality properties of the Gegenbauer functions results in the simple relationship

$$F_j = 4\pi\mu D_{2,j}. \tag{2.16}$$

Equation (2.16) demonstrates, just as for the case of a single sphere, that only the first multipole contributes to the drag forces exerted on each submerged sphere. While the integral (2.15) is performed along the surface of the sphere holding r_j constant the result (2.16) can be easily generalized to any surface drawn in the fluid which encloses the origin of the same multipoles, see Chen & Skalak (1970). Since the stress distribution in Stokes flow is an equilibrium field the forces on two closed surfaces which contain no singularities in the region between them will be the same. Thus, the fact that the truncation procedure provides only an approximation to the actual boundary shape does not affect the drag result if the value of D_{2j} is unchanged.

3. Solutions for two spheres

Solutions using the multipole representation technique to axisymmetric slow viscous flow past two spheres along their line of centres will be presented in this section. This two sphere problem was chosen since the exact solutions presented by Stimson & Jeffery (1926) provide a convenient means for evaluating the truncated multipole representation technique. The solutions for the flow past submerged objects can be presented graphically by plotting streamline patterns and also by calculating the drag force on each object.

Happel & Brenner (1965) describe a convenient coefficient for comparing the

drag on a sphere in an array to the drag on a single sphere. The well-known Stokes result for the drag force on a single sphere is

$$F = 6\pi\mu U a. \tag{3.1}$$

Based on (3.1), λ is defined as follows:

$$F_j = 6\pi\mu U a \lambda_j, \tag{3.2}$$

where j represents the particular sphere in the chain (see figure 1). Referring back to (2.16), we recall that the drag force exerted on a submerged sphere is represented by $F_j = 4\pi\mu D_{2j}$. Combining (2.16) and (3.2) produces

$$\lambda_j = D_{2j}/1{\cdot}5\, Ua. \tag{3.3}$$

In all of the two sphere problems considered herein the sphere radius and the free-stream velocity U have been normalized to unity. Also for the case of two spheres, the drag forces on each of the spheres are equal owing to symmetry and therefore the subscript j will be dropped from λ, i.e. for two spheres

$$\lambda = D_2/1{\cdot}5. \tag{3.4}$$

In writing a program to determine the B_{nj} and D_{nj} constants in (2.11) some practical hints gleaned from the experience of the authors should prove to be useful. The no-slip boundary conditions presented in the previous section are represented by

$$V_{rj} = 0 = \partial\psi/\partial\theta_j,$$
$$V_{\theta j} = 0 = \partial\psi/\partial r_j.$$

Differentiation of the stream function with respect to each sphere individually is tedious as there is a different origin for each sphere and each r_j and θ_j is a function of all the other r_j's and θ_j's. For this reason it is simpler to use a rectangular co-ordinate system which has common co-ordinates for each sphere. The velocities V_{rj} and $V_{\theta j}$ are orthogonal and in the same plane. Therefore all other velocities originating from the same point as V_{rj} and $V_{\theta j}$ and in the same plane must be zero. In particular, V_x and V_y must be identically zero. A simpler set of boundary conditions, equivalent to the above, would therefore be

$$\left.\begin{aligned} V_x &= 0 = \partial\psi/\partial y \\ V_y &= 0 = \partial\psi/\partial x \end{aligned}\right\} \quad \text{on} \quad r_j = a. \tag{3.5}$$

Second, when specifying the number of points along the boundary of each sphere where the conditions (3.5) must be exactly satisfied it is desirable to specify an odd number of points. The reason for this is as follows. The first point that should be specified should always be the highest point on the generating arc (i.e. the point $r_j = a$, $\theta_j = \frac{1}{2}\pi$). This point is most advantageous as the drag on the sphere is a strong function of the projected area of the sphere normal to the direction of flow and the above mentioned point provides the best single estimate of this projected area. The argument is valid for all low aspect ratio objects, e.g. the drag on a flat disk is only 15·2 % lower than the drag on a sphere of the same diameter. If more points along the generating arc are to be specified, they should occur as mirror image pairs about the line $\theta_j = \frac{1}{2}\pi$ in order to satisfy

the geometric symmetry of the boundary about this line. The particular technique used by the authors for spacing these points along each boundary was to divide the half arc of the sphere into equal segments. Using this simple procedure it was found that convergence was rapidly attained in all cases examined. For this reason it was decided that the development of an algorithm for selecting the boundary points more efficiently would not be required.

A practical difficulty arises from the specification of the first point, i.e. $\phi = 0$ or $\theta = \frac{1}{2}\pi$. Referring to equations (2.2) and (2.11), V_{rj} can be represented as follows

$$V_{rj} = -U\cos\theta_j + \sum_j \sum_n [B_{nj} r_j^{-n-1} + D_{nj} r_j^{-n+1}] P_{n-1}(\cos\theta_j). \tag{3.6}$$

It can be seen that if $\theta_j = \frac{1}{2}\pi$ the trivial solution of $0 = 0$ will result when $n = 2$, as $P_1(\cos\theta_j) = \cos\theta_j$. Thus, one of the algebraic equations in the set (2.14) is lost, with the result that one of the elements of the principal diagonal will be equal to zero thereby rendering a solution impossible. In order to overcome this difficulty, the top point can be considered to be a combination of two points that are very close together, i.e. $\phi = \pm\alpha$. The technique used for choosing α is to solve a number of problems in which the boundary conditions are exactly satisfied at the two points $\phi = \pm\alpha$ on each sphere only and noting the largest value of α for which convergence to a prescribed accuracy is obtained. These results are presented in table 1. Examination of table 1 indicates that λ con-

Number of points, M	Spacing, d/a	ϕ	λ
2	1	10°	0·65994
2	1	5°	0·66113
2	1	3°	0·66139
2	1	2°	0·66147
2	1	1°	0·66152
2	1	0·1°	0·66152
2	2	10°	0·74991
2	2	5°	0·75047
2	2	3°	0·75059
2	2	2°	0·75062
2	2	1°	0·75065
2	2	0·1°	0·75065
2	4	10°	0·84587
2	4	5°	0·84599
2	4	3°	0·84602
2	4	2°	0·84603
2	4	1°	0·84604
2	4	0·1°	0·84604
2	8	10°	0·91481
2	8	5°	0·91483
2	8	3°	0·91483
2	8	2°	0·91483
2	8	1°	0·91483
2	8	0·1°	0·91483

TABLE 1. Convergence trials for choosing ϕ for two spheres

verges to five significant figures for all sphere spacings where $|\alpha| \leqslant 1°$. Therefore, in all subsequent multiple sphere problems presented in this study ϕ was taken as 1° for the first two points and these two points were considered to be the single high point required.

A fundamental question that remains unanswered at this point is how many multipoles (or at how many points on the generating arc at which the no-slip condition is exactly satisfied) are required for each sphere in order that a solution of prescribed accuracy will result. The accuracy of the truncation is principally a function of d/a. Thus, the convergence characteristics of the two sphere problem were examined over the entire range of spacings, i.e. $1 \leqslant d/a < \infty$. This problem was handled using the multipole technique satisfying the no-slip boundary condition at varying numbers of points along the generating arc of each sphere. The drag results are shown in table 2.

Number of points, M	Spacing, d/a	λ
1	1	0·66152
3	1	0·64411
5	1	0·64487
7	1	0·64514
9	1	0·64515
11	1	0·64515
1	2	0·75065
3	2	0·74244
5	2	0·74226
7	2	0·74226
1	3	0·80851
3	3	0·80477
5	3	0·80472
7	3	0·80472
1	4	0·84604
3	4	0·84414
5	4	0·84412
7	4	0·84412
1	8	0·91484
3	8	0·91454
5	8	0·91454
1	16	0·95530
3	16	0·95525
5	16	0·95525

TABLE 2. Approach to the exact solution for flow past two spheres

A number of interesting conclusions can be drawn based on the above data. In the most difficult case (i.e. spheres touching) convergence to five significant figures is obtained when the boundary conditions are satisfied at nine equally spaced points on each generating arc. This rapid convergence for the case of two spheres touching is in dramatic contrast to the results of applying the method of reflexions to this same problem. Faxen (1925) (with an appendix by

Dahl) carried computations based on the method of reflexions to the ninth power and obtained an equation for λ. Happel & Brenner (1965) employed an empirical procedure based on the assumption that the last terms in Dahl's expression represent a slowly converging geometric series and obtained the following expression for λ:

$$\lambda = \sum_{n=0}^{9} (-1)^n \alpha_n (a/d)^n. \tag{3.7}$$

Numerical values for α_n are listed by Happel & Brenner (1965). When $(a/d) = 1$, λ calculated from (3.7) is 0·48, representing an error of 25·6 %. Happel & Brenner then assumed that for terms in λ in (3.7) corresponding to $n > 9$,

$$\alpha_n = \text{constant} = \tfrac{1}{3}.$$

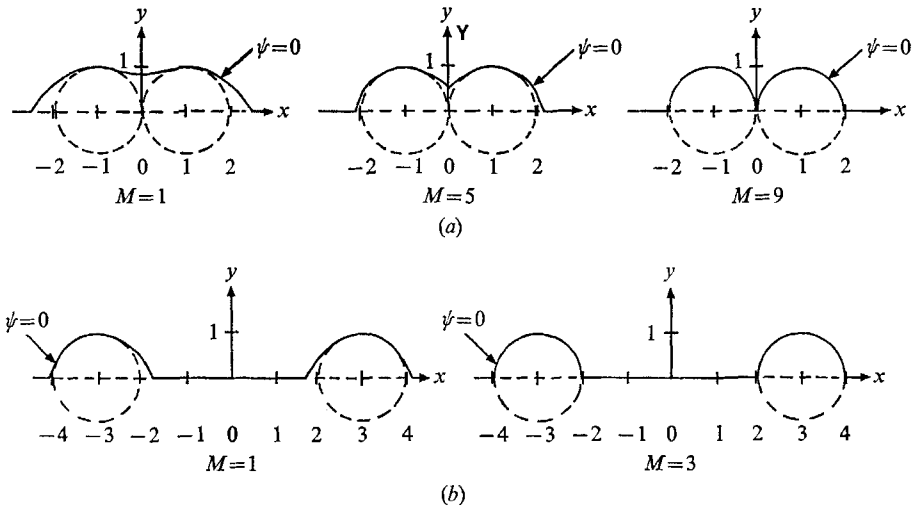

FIGURE 3. Zero streamlines as a function of sphere spacing and number of boundary points M. $d/a = 1, 3$ for (*a*) and (*b*) respectively.

They then carried the summation in (3.7) to infinity and obtained a λ of 0·647 representing an error of 0·31 %. It should be noted that the maximum error resulting from the application of the multipole technique to two touching spheres is 2·5 % when only one point on each generating arc is used. This greatly improved accuracy occurs because the truncation procedure involves simultaneous interactions, even when the lowest order truncation is used. Table 2 indicates that, for each case of two touching spheres convergence to five significant figures is obtained when the boundary conditions are satisfied at nine points along the generating arc of each sphere. For all other cases where $d/a \geqslant 2$, convergence was attained when only five points on each generating arc were used to satisfy the no-slip condition. It is obvious that for any sphere spacing, convergence increases rapidly with increasing numbers of points.

The streamline patterns in figure 3 indicate certain interesting features. For the case where the two spheres are touching and only one point on each generating arc is used to satisfy the no-slip condition it can be seen that the actual solid boundary (represented by the zero streamline) is grossly distorted

from the desired spherical shapes (represented by the broken lines). However, the distorted boundary has the same projected area normal to the direction of flow as the true spherical boundary. This accounts for the fact that the drag on the grossly distorted boundary is only 2·5 % different from the drag on two perfect spheres. This important feature indicates that if drag results are desired, satisfying the boundary conditions at only one point on the generating arc of each sphere will result in a maximum error of 2·5 % whereas if velocity fields are required, a larger number of points on each boundary must be used to eliminate large errors.

Spacing, d/a	Number of points, M	λ	λ exact
1·1276260	1	0·67493	0·65963
	3	0·65932	—
	5	0·65946	—
	7	0·65961	—
	9	0·65963	—
1·5430806	1	0·71431	0·70245
	3	0·70272	—
	5	0·70245	—
	7	0·70245	—
2·3524096	1	0·77408	0·76778
	3	0·76789	—
	5	0·76778	—
	7	0·76778	—
3·7621957	1	0·83843	0·83620
	3	0·83622	—
	5	0·83620	—
	7	0·83620	—
6·1322895	1	0·89221	0·89158
	3	0·89159	—
	5	0·89158	—
	7	0·89158	—
10·067662	1	0·93096	0·93079
	3	0·93079	—
	5	0·93079	—

TABLE 3. Comparison of two sphere solutions with exact results of Stimson & Jeffery

It has been demonstrated that rapid convergence to a solution is possible for all sphere spacings using the new multipole representation technique. The question yet to be answered is whether the solution obtained actually represents the true solution. To this end, a number of solutions to the two sphere problem at various spacings using the multipole technique are compared with the exact solutions of Stimson & Jeffery (1926) in table 3.

These data demonstrate that the solution obtained on convergence using the multipole technique is in fact the exact solution as obtained by Stimson & Jeffery. It is of interest to note that the problem of two touching spheres $d/a = 1$

represents a degenerate case of the exact solution presented by Stimson & Jeffery, i.e.

$$\lambda_{sj} = \tfrac{2}{3}\sinh\alpha \sum_{n=1}^{\infty} \frac{n(n+1)}{(2n-1)(2n+3)}\left[1 - \frac{4\sinh^2(n+\frac{1}{2})\alpha - (2n+1)^2\sinh^2\alpha}{2\sinh(2n+1)\alpha + (2n+1)\sinh 2\alpha}\right], \quad (3.8)$$

where α is defined by $\cosh\alpha = d/a$.

Faxen (1927) developed an integral technique for treating the limiting case of equation (3.8) when $d/a = 1$. The result of applying Faxen's method to the problem of two touching spheres is reported by Goldman, Cox & Brenner (1966) as $\lambda_{sj} = 0{\cdot}6451408$. This result is in fairly close agreement with the equivalent converged solution for λ calculated by the multipole technique and reported in table 2, i.e. $\lambda = 0{\cdot}64515$.

4. Solutions for multiple spheres

In the previous section solutions for the axisymmetric flow past two spheres based on the multipole truncation technique have been presented and were shown to be in agreement with the exact solutions presented by other workers. This section will examine the solutions of the problem of axisymmetric flow past finite chains of spheres. To the best of the authors' knowledge exact solutions for finite chains of three or more spheres do not exist in the literature. This is due to the fact that for assemblages of more than three settling spheres, orientations other than sedimentation along the line of centres appear to represent more stable configurations. Slack & Matthews (1961) have shown experimentally that clusters containing no more than six spheres will tend to arrange themselves in the same horizontal plane at the vertices of a regular polygon. The purpose of considering linear chains of more than three spheres is to demonstrate the application and convergence characteristics of this new technique for systems containing three or more spheres rather than to infer that such chains represent stable settling configurations.

Solutions to flow past chains containing 3, 5, 7, 9, 11, 13, 15 and 101 equally spaced spheres where the boundary conditions are satisfied at one or more points on each generating arc have been obtained. The results of the preceding section for two spheres provide a qualitative guide to the accuracy of these solutions. The maximum error to be expected in λ_j (when the spheres are touching and the boundary conditions are satisfied at only the $\theta_j = \frac{1}{2}\pi$ point on the generating arc) will be approximately $2\frac{1}{2}\%$. The maximum error will be greatly reduced if more than one point is chosen, e.g. for three points on each generating arc the probable error when the spheres are touching will be $0{\cdot}16\%$.

In order to handle the 15 sphere problem utilizing only the two lowest order multipoles, 60 linear simultaneous equations need to be solved as the uppermost point is actually two points $\phi = \pm 1°$ and this involves four velocity boundary conditions for each sphere. Although this is accomplished very rapidly with the use of a computer the storage capacity required is rather high. In order to increase the number of spheres from 15 to say 101 it is necessary for 404 simultaneous equations to be solved. This is not difficult but requires the use of complex

overlaying techniques to accommodate the entire coefficient matrix in core (i.e. 163216 words of storage or 652864 bytes are required).

The drag correction factor λ_j was determined for chains containing various numbers of spheres at different sphere spacings in the range $1 \leqslant d/a \leqslant 16$, with the boundary conditions satisfied at both one and three points on each generating arc. The results for $d/a = 2$ are plotted in figure 4. The values for λ_j for the central spheres in a 101 sphere chain are also shown. It is estimated that the error in λ_j where the boundary conditions are satisfied at one point on each

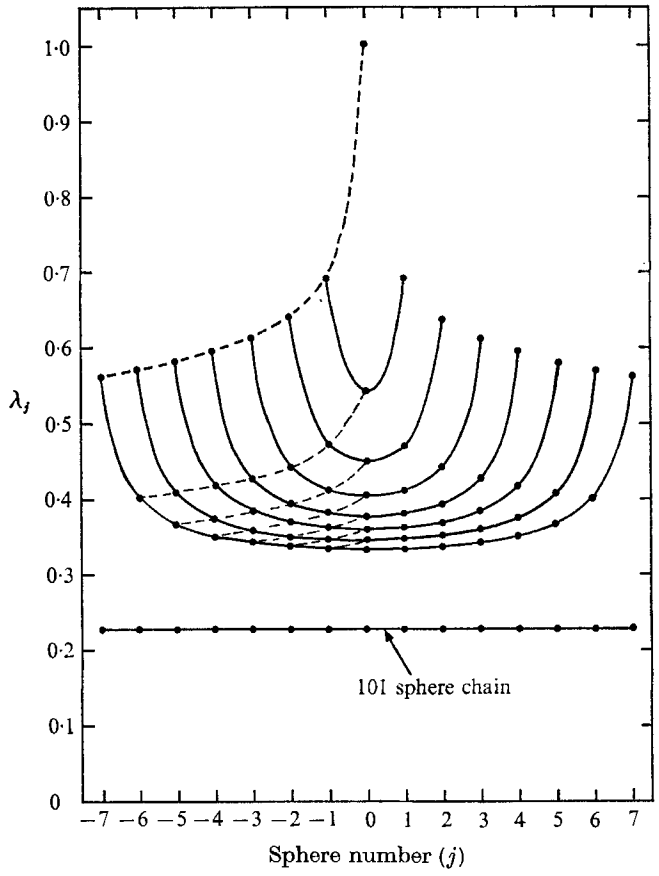

FIGURE 4. Drag coefficient factor λ_j for chains containing different numbers of spheres with $d/a = 2$.

generating arc will be approximately 1·1 % based on the results of the previous section. Although the drag correction factor λ_j has a discrete value for each object the values have been connected by solid lines to indicate each individual chain. It can be seen that as the chain length is increased the drag on the central sphere decreases indicating a shielding effect. As the ends of any chain are approached the relative drag on adjacent spheres changes rapidly, demonstrating the importance of end effects. As the length of the chain increases, the drag on the spheres located in the central portion of the chain changes very

slowly. In the limit of an infinite chain the drag on each sphere would be the same.

The broken lines indicate the drag on the nth sphere in any chain. It can be seen that as the chain length increases, the broken lines tend to become horizontal, once again demonstrating the relatively strong shielding characteristics exhibited by a chain of spheres.

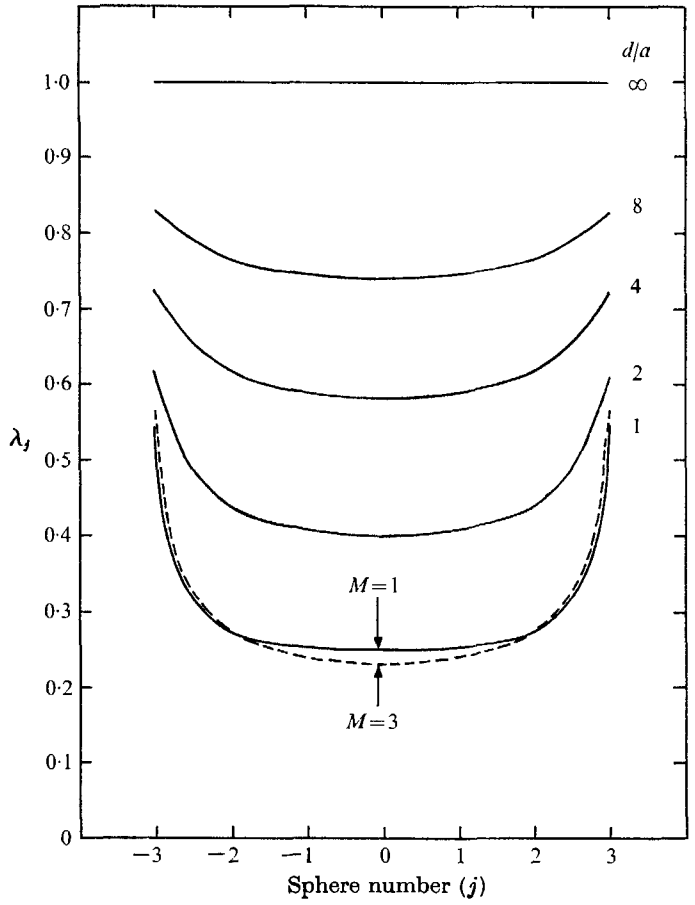

FIGURE 5. Drag correction factor for a seven sphere chain at different sphere spacings.

All the above results apply only to a spacing (d/a) of 2. In order to determine the effect of sphere spacing on λ_j, curves of λ_j *vs.* sphere number with d/a as a parameter were plotted for a chain of 7 spheres in figure 5. These results demonstrate that as the spacing increases the end effects will decrease. Also, as the spheres get closer together the drag on each sphere in the chain will be reduced. In §§6 and 7 the drag on multiple prolate and oblate spheroids in a chain will be compared with these results for multiple spheres.

Figure 6 represents plots of the drag correction factor λ_j versus the sphere number in a chain containing 101 spheres at spacings (d/a) of 1, 2 and 4. For all cases the boundary conditions were satisfied at one point ($\theta_j = \frac{1}{2}\pi$) on each

sphere with probable errors of $2\frac{1}{2}$ % for the case of $d/a = 1$ and 0·2 % for $d/a = 4$. This figure indicates that the drag on all the spheres in the central section of the chain changes very little with position. However, it is interesting to note the extent of the end effects exhibited by long finite chains as shown in figure 6.

Finally, if equations (2.11) and (3.3) are used to determine the drag on each sphere in a chain of infinite extent in an unbounded fluid (using the property of perfect periodicity, i.e. $B_{nj} = B_n$ and $D_{nj} = D_n$), it is found that λ_j approaches zero as the number of spheres in the chain becomes very large. This paradoxical result is in contrast to the results of Wang & Skalak (1969), who considered the case of an infinite chain of spheres moving along the axis of a circular cylinder.

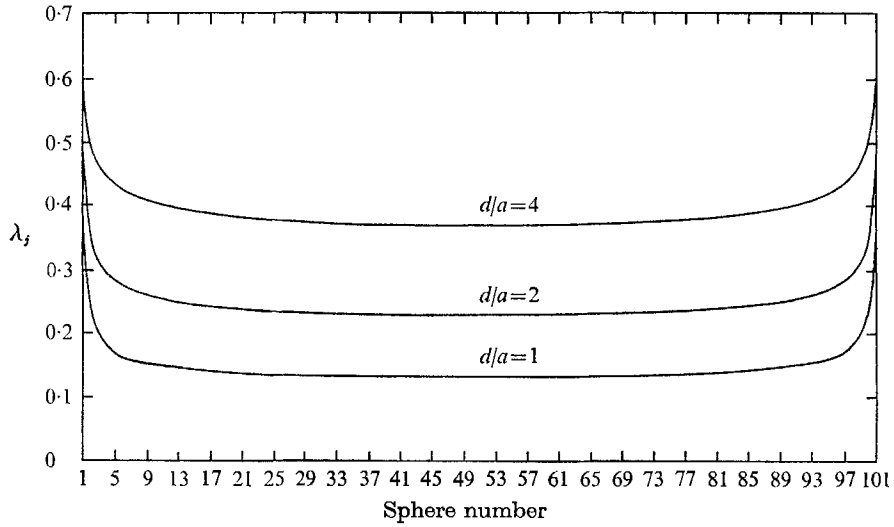

FIGURE 6. Drag correction factor for a 101 sphere chain at different sphere spacings.

These workers found that for the case of an infinite chain of touching spheres having a ratio of sphere diameter to cylinder diameter of 0·1, the correction to the Stokes drag would be 0·473. This zero drag is in accord with Burgers approximate formula for calculating the drag force per unit length on long cylinders:

$$F/h = 2\pi\mu U/(\ln(h/r_n) - 0{\cdot}72), \tag{4.1}$$

where h = cylinder length, r_n = cylinder radius. It can be seen from (4.1) that as h tends to infinity the drag force per unit length on the cylinder approaches zero.

5. Formulation for bifocal objects

In this section the formulation of a general solution for creeping motion past a finite chain of equally spaced bifocal objects will be presented. An important class of objects in this category are prolate (ovary) spheroids and oblate (planetary) spheroids. (It should be kept in mind that oblate spheroids are only bifocal in a meridian plane as the locus of their foci form a circular ring about their

minor axis.) The formulation of the general solution in spheroidal co-ordinates of the creeping motion equations (2.1) has been presented by Sampson (1891):

$$\begin{aligned}\psi = {} & 2c^2UI_2(p)\,I_2(q)+[D_2p+B_2H_2(p)+D_4H_4(p)]\,I_2(q)\\ & +[D_3+B_3H_3(p)+D_5H_5(p)]\,I_3(q)\\ & +\sum_{n=4}^{\infty}[D_nH_{n-2}(p)+B_nH_n(p)+D_{n+2}H_{n+2}(p)]\,I_n(q),\end{aligned}\tag{5.1}$$

where U = free-stream velocity, D_n, B_n = constants, $I_n(q)$, $H_n(p)$ = Gegenbauer functions of the first and second kind respectively defined in §2. The p and q are related to the appropriate bifocal co-ordinate transformations (also see figure 7). For prolate spheroids the co-ordinate transformation used is

$$\left.\begin{aligned}&x+iy = c\cosh(\xi+i\eta),\\ &x = c\cosh\xi\cos\eta,\quad y = c\sinh\xi\sin\eta,\\ &p = \cosh\xi = (R_1+R_2)/2c,\quad q = \cos\eta = (R_2-R_1)/2c,\\ &R_1 = [(x-c)^2+y^2]^{\frac{1}{2}},\quad R_2 = [(x+c)^2+y^2]^{\frac{1}{2}},\\ &x^2/a^2+y^2/b^2 = 1,\quad c^2 = a^2-b^2,\end{aligned}\right\}\tag{5.2}$$

while for oblate spheroids the co-ordinate transformation used is

$$\left.\begin{aligned}&x+iy = c\sinh(\xi+i\eta),\\ &x = c\sinh\xi\cos\eta,\quad y = c\cosh\xi\sin\eta,\\ &p = i\sinh\xi = i[((R_1+R_2)/2c)^2-1]^{\frac{1}{2}},\quad q = \cos\eta = [1-((R_2-R_1)/2c)^2]^{\frac{1}{2}},\\ &R_1 = [x^2+(y-c)^2]^{\frac{1}{2}},\quad R_2 = [x^2+(y+c)^2]^{\frac{1}{2}},\\ &x^2/a^2+y^2/b^2 = 1,\quad c^2 = b^2-a^2.\end{aligned}\right\}\tag{5.3}$$

It can be shown that the first term in (5.1) represents the free-stream contribution to the stream function,

$$2c^2UI_2(p)\,I_2(q) = \tfrac{1}{2}Uy^2.$$

Sampson applied (5.1) to the problem of flow past a single spheroid and showed that the following results must be true to produce finite velocities in the far flow field:

$$B_3 = B_4 = B_5 = \ldots = B_n = D_3 = D_4 = \ldots D_n = 0.\tag{5.4}$$

The remaining constants B_2 and D_2 are determined by applying the no-slip boundary conditions

$$V_p = 0 = \partial\psi/\partial q,\quad V_q = 0 = \partial\psi/\partial p,\quad \text{on}\quad p = p_0,\tag{5.5}$$

where p_0 is the surface of the spheroid. Equation (5.1) subject to (5.4) and (5.5) reduces to the solution for the flow past a single spheroid,

$$\psi = 2c^2UI_2(q)\left[I_2(p)-\frac{p+(p_0^2+1)\,H_2(p)}{2(\frac{1}{4}(p_0^2+1)\ln((p_0+1)/(p_0-1))-\frac{1}{2}p_0)}\right].$$

The above solution for a single spheroid is the same as that proposed by Payne & Pell (1960) and Happel and Brenner (1965).

In order to extend Sampson's results for flow past a single spheroid to the case of multiple spheroids the linearity of the equation of motion is used,

$$\psi = \sum_{j=-\frac{1}{2}(N-1)}^{\frac{1}{2}(N-1)} \psi_j, \tag{5.6}$$

where ψ_j is represented by (5.1). Figure 7 shows the geometry of the system.

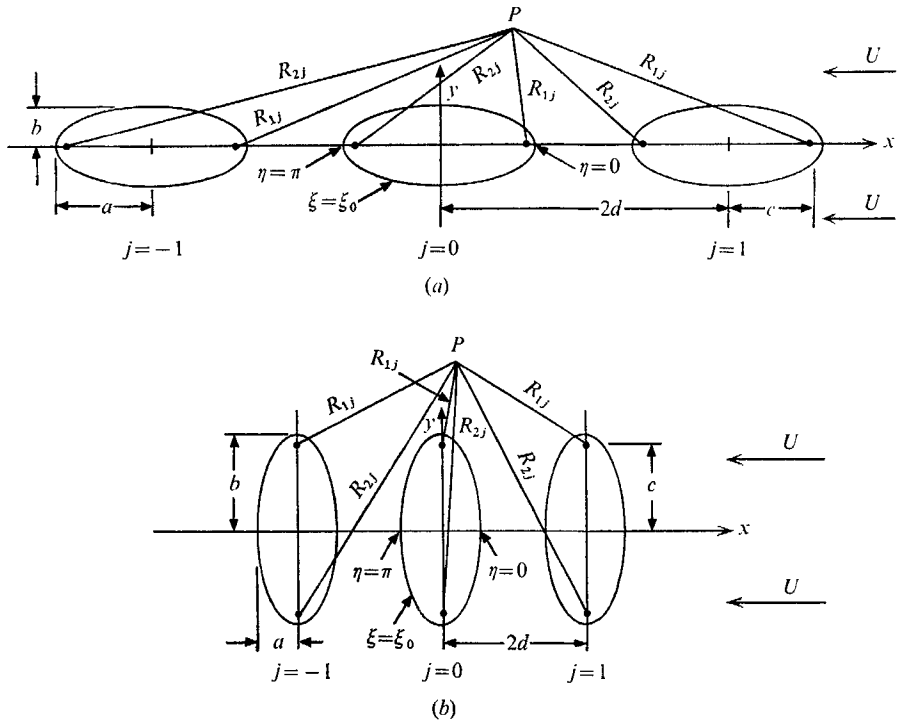

FIGURE 7. Geometry of multiple prolate (*a*) and oblate (*b*) spheroidal systems.

Applying (5.6) to (5.1) one obtains the general form of the solution for the stream function for flow past N spheroids.

$$\begin{aligned}\psi = 2c^2UI_2(p)\,I_2(q) + \sum_{j=-\frac{1}{2}(N-1)}^{\frac{1}{2}(N-1)} \{&[D_{2j}p_j + B_{2j}H_2(p_j) + D_{4j}H_4(p_j)]\,I_2(q_j) \\ &+ [D_{3j} + B_{3j}H_3(p_j) + D_{5j}H_5(p_j)]\,I_3(q_j) \\ &+ \sum_{n=4}^{\infty} [D_{nj}H_{n-2}(p_j) + B_{nj}H_n(p_j) + D_{n+2,j}H_{n+2}(p_j)]\,I_n(q_j)\},\end{aligned} \tag{5.7}$$

where p_j and q_j are defined using (5.2) and (5.3) for each spheroid. For prolate spheroids

$$p_j = (R_{1j} + R_{2j})/2c, \quad q_j = (R_{2j} - R_{1j})/2c$$

and $$R_{1j} = [(x - c - 2jd)^2 + y^2]^{\frac{1}{2}}, \quad R_{2j} = [(x + c - 2jd)^2 + y^2]^{\frac{1}{2}}.$$

For oblate spheroids

$$p_j = i[((R_{1j}+R_{2j})/2c)^2-1]^{\frac{1}{2}}, \quad q_j = [1-((R_{2j}-R_{1j})/2c)^2]^{\frac{1}{2}}$$

and $$R_{1j} = [(x-2jd)^2+(y-c)^2]^{\frac{1}{2}}, \quad R_{2j} = [(x-2jd)^2+(y+c)^2]^{\frac{1}{2}}.$$

As for the case of multiple spheres, (5.7) contains a double series expansion which is infinite in one dimension and can be large in the other. Examination of (5.7) indicates that the multipole truncation technique described in § 2 for multiple spheres is equally valid and readily applied to multiple spheroids. Each term in the inner summation can be interpreted as a multi-lobular disturbance emanating from the geometric centre of the spheroid with its amplitude related to the B_{nj}

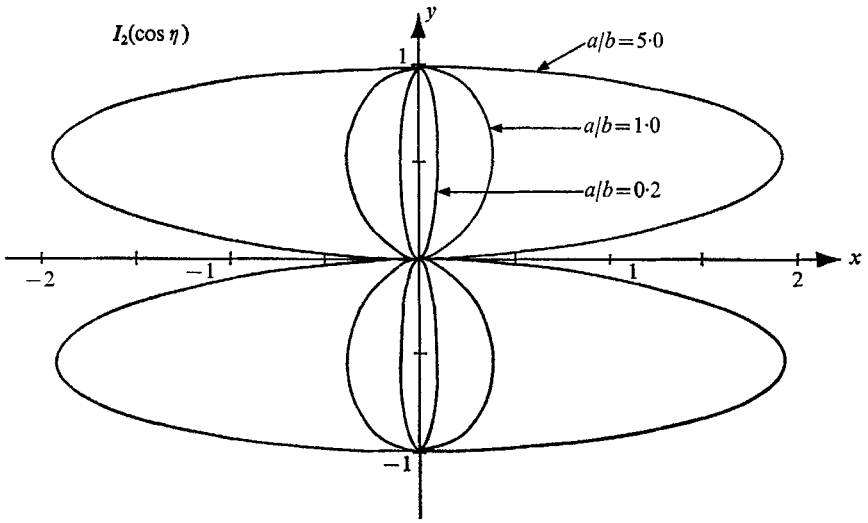

FIGURE 8. Effect of lobe stretching and compression on $I_2(\cos\eta)$.

and D_{nj} coefficients and its angular dependence given by the Gegenbauer function $I_n(q_j)$. The multi-lobular function $I_n(\cos\eta_j)$ differs from the $I_n(\cos\theta_j)$ used in (2.11) for describing spheres in that the angular co-ordinate θ_j allows the lobes of the Gegenbauer functions to conform to natural spherical co-ordinates whereas the q_j co-ordinate stretches or compresses the lobes so as to conform to natural spheroidal co-ordinates. This transformation from θ_j to η_j is shown in figure 8 for the function $I_2(\cos\eta)$ for aspect ratios a/b of 5·0, 1·0 and 0·2. It can be seen that for $a/b = 1{\cdot}0$, $I_2(\cos\eta) = I_2(\cos\theta)$, i.e. the case of a perfect sphere. As the aspect ratio increases above 1·0 an elongation in the x direction occurs and the lobes conform to prolate spheroids. For aspect ratios less than 1·0 compression in the x direction provides lobes that conform to oblate spheroidal cross-sections. Similar results are obtained for the higher order $I_n(q_j)$ and represent a stretching of the diagrams shown in figure 2. All the theory developed in § 2 concerning the use of the multipole truncation technique for flow past spheres can be applied to the flow past spheroids. Each multipole contains two arbitrary constants B_{nj} and D_{nj} and thus provides freedom to satisfy the no-slip boundary conditions at one point along the generating arc of each spheroid.

To satisfy the no-slip conditions exactly over the entire surface of each spheroid would require the use of an infinite number of multipoles. For any point m on the generating arc of a spheroid in a chain containing N spheroids the no-slip boundary conditions can be represented as follows for $p_{jm} = p_{0jm}$ and $q_{jm} = q_{jm}$.

$$\left.\begin{aligned} V_{pjm} = 0 = A'_{jm} + \sum_{s=1}^{N} \{&[D'_{2,s,m} D_{2,s} + B'_{2,s,m} B_{2,s}] \\ &+ [D'_{3,s,m} D_{3,s} + B'_{3,s,m} B_{3,s}] + \sum_{n=4}^{M+1} [D'_{n,s,m} D_{n,s} + B'_{n,s,m} B_{n,s}]\}, \\ V_{q,jm} = 0 = A''_{jm} + \sum_{s=1}^{N} \{&[D''_{2,s,m} D_{2,s} + B''_{2,s,m} B_{2,s}] \\ &+ [D''_{3,s,m} D_{3,s} + B''_{3,s,m} B_{3,s}] + \sum_{n=4}^{M+1} [D''_{n,s,m} D_{n,s} + B''_{n,s,m} B_{n,s}]\}, \end{aligned}\right\} \quad (5.8a)$$

for $1 \leqslant m \leqslant M$.

$$\left.\begin{aligned} A'_{jm} &= -2c^2 U I_2(p_{jm}) P_1(q_{jm}), \\ B'_{nsm} &= -Q_{n-1}(p_{sm}) I_n(q_{sm}) \partial p_{sm}/\partial q_{jm} - H_n(p_{sm}) P_{n-1}(q_{sm}) \partial q_{sm}/\partial q_{jm}, \\ D'_{2,s,m} &= I_2(q_{sm}) \partial p_{sm}/\partial q_{jm} - p_{sm} P_1(q_{sm}) \partial q_{sm}/\partial q_{jm}, \\ D'_{3,s,m} &= -P_2(q_{sm}) \partial q_{sm}/\partial q_{jm}, \\ D'_{nsm} &= -[Q_{n-3}(p_{sm}) I_n(q_{sm}) + Q_{n-1}(p_{sm}) I_{n-2}(q_{sm})] \partial p_{sm}/\partial q_{jm} \\ &\quad -[H_{n-2}(p_{sm}) P_{n-1}(q_{sm}) + H_n(p_{sm}) P_{n-3}(q_{sm})] \partial q_{sm}/\partial q_{jm}, \\ A''_{jm} &= -2c^2 U P_1(p_{jm}) I_2(q_{jm}), \\ B''_{nsm} &= -Q_{n-1}(p_{sm}) I_n(q_{sm}) \partial p_{sm}/\partial p_{jm} - H_n(p_{sm}) P_{n-1}(q_{sm}) \partial q_{sm}/\partial p_{jm}, \\ D''_{2,s,m} &= I_2(q_{sm}) \partial p_{sm}/\partial p_{jm} - p_{sm} P_1(q_{sm}) \partial q_{sm}/\partial p_{jm}, \\ D''_{3,s,m} &= -P_2(q_{sm}) \partial q_{sm}/\partial p_{jm}, \\ D''_{nsm} &= -[Q_{n-3}(p_{sm}) I_n(q_{sm}) + Q_{n-1}(p_{sm}) I_{n-2}(q_{sm})] \partial p_{sm}/\partial p_{jm} \\ &\quad -[H_{n-2}(p_{sm}) P_{n-1}(q_{sm}) + H_n(p_{sm}) P_{n-3}(q_{sm})] \partial q_{sm}/\partial p_{jm}, \end{aligned}\right\} \quad (5.8b)$$

where M is the total number of points on each generating arc where the no-slip boundary conditions are to be satisfied.

It can be seen that (5.8a) and (5.8b) are the equivalent equations in spheroidal co-ordinates to (2.13a) and (2.13b) in spherical co-ordinates. Therefore, the solution to slow viscous flow past N submerged spheroids where the boundary conditions are satisfied at M points on each generating arc is represented explicitly by the matrix equation (2.14) where each element is given by (5.8b).

It is of interest to note that (5.7) reduces to the solution for flow past equally spaced multiple spheres as the distance between the foci of the spheroids approaches zero. The proof will be outlined for the case of prolate spheroids ($p_j = \cosh \xi_j$) with the free-stream contribution in (5.7) represented as

$$\tfrac{1}{2} U r_0^2 \sin^2 \theta_0.$$

A similar proof could be presented for the case of oblate spheroids. Consider the repeating term in (5.7)

$$R_{nj} = D_{nj} H_{n-2}(p_j) + B_{nj} H_n(p_j) + D_{n+2,j} H_{n+2}(p_j).$$

Using the recurrence relationship

$$H_{n+2}(p_j) = ((p_j^2 - \epsilon_n)/\delta_n) H_n(p_j) - (\xi_n/\delta_n) H_{n-2}(p_j),$$

where $$\xi_n = (n-2)(n-3)/(2n-1)(2n-3), \quad \xi_0 = \xi_1 = 0,$$

$$\delta_n = (n+1)(n+2)/(2n-1)(2n+1), \quad \epsilon_n = (2n^2-2n-3)/(2n+1)(2n-3),$$

results in
$$R_{nj} = E_{nj} H_{n-2}(p_j) + F_{nj} H_n(p_j) + G_{nj} p_j^2 H_n(p_j), \tag{5.9}$$

where
$$E_{nj} = D_{nj} - (\xi_n/\delta_n) D_{n+2,j},$$
$$F_{nj} = B_{nj} - (\epsilon_n/\delta_n) D_{n+2,j},$$
$$G_{nj} = D_{n+2,j}/\delta_n.$$

As $r_j = [(x-2jd)^2 + y^2]^{\frac{1}{2}}$ it is simple to show that as $c \to 0$, $p_j \to r_j/c$, i.e.

$$H_n(p_j) \to H_n(r_j/c).$$

For large values of the argument the asymptotic behaviour of Gegenbauer functions of the second kind can be deduced from their relationship to the hypergeometric function,

$$H_n(p) = 2^{-n}((n-2)!\,\pi^{\frac{1}{2}}/(n-\tfrac{1}{2})!)\, p^{-n+1} F[\tfrac{1}{2}(n-1), \tfrac{1}{2}n, n-\tfrac{1}{2}, (p^{-2})],$$

i.e.
$$H_n(r_j/c) \to M_n (r_j/c)^{-n+1} \quad \text{as} \quad c \to 0,$$

since
$$F[\tfrac{1}{2}(n-1), \tfrac{1}{2}n, n-\tfrac{1}{2}, (p^{-2})] \to 1 \quad \text{as} \quad c \to 0,$$

where M_n is a constant and can therefore be combined with c to produce

$$H_n(r_j/c) \to M'_n r_j^{-n+1} \quad \text{as} \quad c \to 0. \tag{5.10}$$

Combining (5.10) with (5.9) results in

$$R_{nj} \to E'_{nj} r_j^{-n+3} + F'_{nj} r_j^{-n+1} \quad \text{as} \quad c \to 0.$$

Using this result with (5.10) in (5.7) produces

$$\psi = \tfrac{1}{2} U r_0^2 \sin^2\theta_0 + \sum_j \{[D'_{2j} r_j + B'_{2j} r_j^{-1}] I_2(q_j) + [D'_{3j} + B'_{3j} r_j^{-2}] I_3(q_j) + \sum_{n=4}^{\infty} [E'_{nj} r_j^{-n+3} + F'_{nj} r_j^{-n+1}] I_n(q_j)\}.$$

It can be seen that this is identical in form to (2.11), the solution to the stream function for flow past multiple spheres.

Finally, one wishes to determine the drag force exerted by the fluid on each submerged spheroid. In this case, instead of using the integral relationship to determine F_j, a technique developed by Payne & Pell (1960) will be used. The above authors have shown that provided that the fluid at infinity is at rest the drag on a submerged object can be represented as follows:

$$F_j = 8\pi\mu \lim_{r_j \to \infty} (r_j \psi / r_j^2 \sin^2\theta_j). \tag{5.11}$$

If the fluid at infinity is not at rest (5.11) can easily be modified to represent the drag force

$$F_j = 8\pi\mu \lim_{r_j \to \infty} (r_j (\psi - \psi_\infty)/r_j^2 \sin^2\theta_j). \tag{5.12}$$

For the case of prolate spheroids

$$r_j = c(\cosh^2\xi_j\cos^2\eta_j + \sinh^2\xi_j\sin^2\eta_j)^{\frac{1}{2}},$$

and as $$r_j\to\infty, \quad r_j\to c\cosh\xi_j\to ce^{\xi_j},$$

i.e. $$\cosh\xi_j\to\sinh\xi_j \quad \text{for} \quad \xi\gg 1.$$

Also $$r_j^2\sin^2\theta_j = y^2 = c^2\sinh^2\xi_j\sin^2\eta_j,$$

and as $$r_j\to\infty, \quad r_j^2\sin^2\theta_j\to c^2e^{2\xi_j}\sin^2\eta_j,$$

i.e. $$r_j/r_j^2\sin^2\theta_j\to 1/ce^{\xi_j}\sin^2\eta_j \quad \text{for} \quad \xi_j\gg 1.$$

Using the fact that $$\psi_\infty = 2c^2UI_2(p_0)I_2(q_0),$$

(5.12) reduces to $$F_j = 8\pi\mu \lim_{ce^{\xi_j}\to\infty} (\psi-\psi_\infty)/ce^{\xi_j}\sin^2\eta_j. \tag{5.13}$$

It has already been demonstrated that for large arguments the asymptotic behaviour of Gegenbauer functions of the second kind can be represented as follows

$$\left.\begin{aligned} H_n(p_j)&\to p_j^{-n+1} \quad \text{as} \quad p_j\to\infty,\\ H_n(p_j)&\to 1/e^{n\xi_j-\xi_j} \quad \text{as} \quad r_j\to\infty.\end{aligned}\right\} \tag{5.14}$$

Applying (5.14) and (5.7) to (5.13) it can be seen that the only multipole in (5.7) that contributes to the drag is the first one,

$$\left.\begin{aligned} &\frac{p_jI_2(q_j)}{ce^{\xi_j}\sin^2\eta_j}\to\frac{\frac{1}{2}e^{\xi_j}\sin^2\eta_j}{ce^{\xi_j}\sin^2\eta_j}\to\frac{1}{2c} \quad \text{as} \quad \xi_j\to\infty,\\ &\frac{I_3(q_j)}{ce^{\xi_j}\sin^2\eta_j}\to 0, \quad \frac{H_2(p_j)I_2(q_j)}{ce^{\xi_j}\sin^2\eta_j}\to\frac{1}{2ce^{2\xi_j}}\to 0 \quad \text{as} \quad \xi_j\to\infty.\end{aligned}\right\} \tag{5.15}$$

Using (5.15) the following result for the drag on each object is obtained:

$$F_j = 4\pi\mu D_{2j}/c. \tag{5.16}$$

Thus, as was the case for submerged spheres, the drag is determined by the intensity of the first-order multipole in the expression for the stream function. This intensity of course depends implicitly on the higher order multipoles as D_{2j} is just one element of the set of matrix equations which are solved simultaneously. By adopting similar techniques it can be shown that (5.16) applies to the case of oblate spheroids as well as to prolate spheroids.

In order to be able to compare drag results for spheroids with the Stokes drag for a single sphere, the following argument is proposed. Consider a sphere having a radius equal to the axis dimension of the spheroid normal to the direction of flow. This would be represented by the minor axis of a prolate spheroid or the major axis of an oblate spheroid – in both cases represented by the symbol b in this study. The drag on a perfect sphere of radius b as represented by Stokes formula would be

$$F = 6\pi\mu Ub. \tag{5.17}$$

If, once again, λ_j is used to represent the correction to the Stokes drag on a single sphere in terms of the drag force on a spheroid, (5.17) can be modified to

$$F_j = 6\pi\mu Ub\lambda_j. \tag{5.18}$$

Solving (5.18) and (5.16) simultaneously results in the following expression for λ_j

$$\lambda_j = D_{2j}/1{\cdot}5\, cbU. \tag{5.19}$$

6. Solutions for multiple prolate spheroids

Creeping motion solutions for flow past two spheroids have been formulated by Wakiya (1965). Although these general solutions were formulated for any orientation of the spheroids they were not solved for the axisymmetric case and cannot therefore be used as a source of comparison for the results presented in this section.

Before presenting solutions for flow past prolate spheroids some of the practical aspects of solving equations (5.8) will be discussed. The major numerical difficulty is that ill conditioning can occur in the matrix equation (2.14) if any of the p_j arguments become large or if high order multipoles are required to satisfy the boundary conditions at many points on each generating arc, as the absolute values of Gegenbauer functions of the second kind $H_n(p_j)$ become extremely small for large arguments as well as for high orders. When ill conditioning exists instead of using a direct matrix reduction technique one employs an iterative matrix reduction scheme (i.e. corrections to original solution computed from residual vectors) utilizing double precision arithmetic. A second difficulty which is not immediately obvious is associated with the generation of Gegenbauer and Legendre functions of the second kind using recurrence relationships of the form

$$Q_n(p) = ((2n-1)\,pQ_{n-1}(p) - (n-1)\,Q_{n-2}(p))/n$$

and

$$H_n(p) = (Q_{n-2}(p) - Q_n(p))/(2n-1).$$

Even the use of double precision arithmetic produces errors in $H_{10}(10)$, computed from the above of $O(10^{15})$. Therefore, when the absolute value of either $Q_n(p)$ or $H_n(p)$ is less than 10^{-9} the values of these functions should be calculated directly from their asymptotic behaviour rather than the above recurrence relationships. The asymptotic behaviour of these functions for $p \gg 1$ is given by

$$Q_n(p) = (n!/1.3.5.7...(2n+1))\,p^{-n-1},$$

$$H_n(p) = ((n-2)!/1.3.5.7...(2n-1))\,p^{-n+1}.$$

A third difficulty, discussed previously for multiple spheres, is that the equations (5.8*a*) reduce to trivial form at $\phi = 0$, the point located vertically above the geometric centre of the spheroid. This uppermost point must again be represented by two points on the generating arc of each spheroid where the no-slip conditions are to be satisfied, and be chosen so that the equation for these two points converges to the solution for a single point. The results of these particular convergence trials will not be presented in detail. It is sufficient to state that in all cases examined the value of the angle $\phi = \pm\alpha$ in degrees required to produce convergence to five significant figures was equal in magnitude to the ratio of major to minor axis, $\alpha = a/b$.

In order to show that (5.7) converges to the exact solution for the flow past a single prolate spheroid, solutions were obtained for two prolate spheroids having

a spacing to major axis ratio of 10 000. The boundary conditions were satisfied at the uppermost point on each generating arc only. These results, based on the two lowest order multipoles, are compared with the exact solutions of Happel & Brenner (1965) in table 4. All results in this section will be stated in terms of the drag correction factor λ_j defined by (5.19).

Aspect ratio, a/b	Spacing, d/a	λ, equation (5.7)	λ, Happel & Brenner
1·01	10 000	1·002	1·002
1·10	10 000	1·020	1·020
1·50	10 000	1·102	1·102
2·00	10 000	1·204	1·204
5·00	10 000	1·785	1·785
10·00	10 000	2·647	2·647
100·00	10 000	13·895	13·895

TABLE 4. Comparison of drag results for one prolate spheroid from (5.7) with exact results of Happel & Brenner (1965)

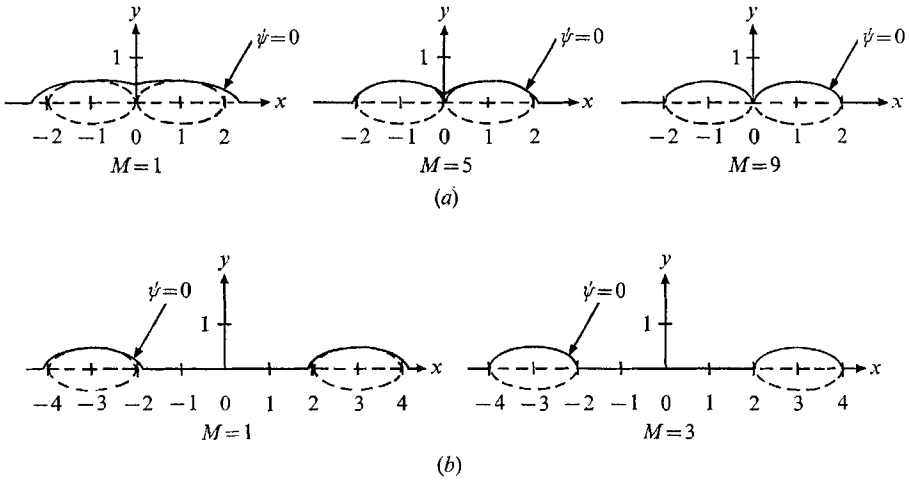

FIGURE 9. Zero streamlines as a function of spheroid spacing and number of boundary points M for prolate spheroids. $a/b = 2$, (*a*) $d/a = 1$, (*b*) $d/a = 3$.

Table 4 demonstrates that in the limit of one prolate spheroid, (5.7) agrees with the exact solution to four significant digits. We next examine the convergence characteristics of truncated multipole solutions for flow past two prolate spheroids at various spacings where the boundary conditions are satisfied at increasing numbers of points along the generating arc of each spheroid. The locations of these boundary points were chosen by dividing the η co-ordinate into equal parts. These results are presented in table 5. The streamlines have also been plotted in figure 9 for certain cases of particular interest.

Table 5 indicates that convergence to five significant figures is rapidly attained in all cases – even when the spheroids are touching. Except for the case of two spheroids touching where seven points were required for five digit convergence, only five points on each object resulted in convergence to five

significant figures for all other spacings. It can be seen that the relative errors in λ_j are almost the same as those for the two sphere problem. The distortions of the zero streamline for two touching spheroids ($a/b = 2$) and for two spheroids having a d/a ratio of three (see figure 9) are similar to the distortions in the case of two spheres but of smaller magnitude. This result is not unexpected

Aspect ratio, a/b	Spacing, d/a	Number of boundary points, M	λ
2·0	1·0	1	0·8669
2·0	1·0	3	0·8452
2·0	1·0	5	0·8441
2·0	1·0	7	0·8442
2·0	1·0	9	0·8442
2·0	2·0	1	0·9876
2·0	2·0	3	0·9813
2·0	2·0	5	0·9812
2·0	3·0	1	1·0480
2·0	3·0	3	1·0458
2·0	3·0	5	1·0458
2·0	4·0	1	1·0825
2·0	4·0	3	1·0815
2·0	4·0	5	1·0815
2·0	8·0	1	1·1397
2·0	8·0	3	1·1396
2·0	8·0	5	1·1396
2·0	16·0	1	1·1709
2·0	16·0	3	1·1709
5·0	1·0	1	1·4076
5·0	1·0	3	1·3752
5·0	1·0	5	1·3705
5·0	1·0	7	1·3700
5·0	1·0	9	1·3700
5·0	1·0	11	1·3700
5·0	2·0	1	1·5727
5·0	2·0	3	1·5676
5·0	2·0	5	1·5675
5·0	2·0	7	1·5675
5·0	2·0	9	1·5675
5·0	3·0	1	1·6380
5·0	3·0	3	1·6365
5·0	3·0	5	1·6364
5·0	3·0	7	1·6364
5·0	4·0	1	1·6726
5·0	4·0	3	1·6719
5·0	4·0	5	1·6719
5·0	8·0	1	1·7270
5·0	8·0	3	1·7269
5·0	8·0	5	1·7269
5·0	16·0	1	1·7554
5·0	16·0	3	1·7554

TABLE 5. Convergence of drag results for two prolate spheroids

because, as the aspect ratio increases, the objects become extended in the flow direction and in the limit of infinite aspect ratio the boundaries will be parallel to the free-stream streamlines.

Finally drag results for flow past chains consisting of from one to fifteen prolate spheroids have been plotted in figure 10. The spheroids considered for this case had an aspect ratio of five and a spacing parameter (d/a) of two. The drag correction factor λ_j for each spheroid in each chain has been plotted against

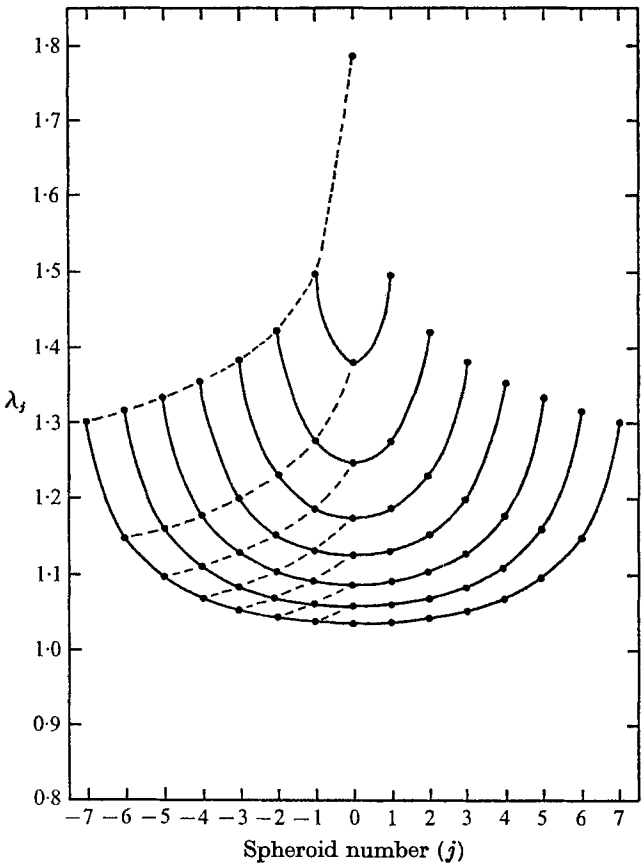

FIGURE 10. Drag correction factor λ_j for chains containing different numbers of prolate spheroids with $a/b = 5{\cdot}0$, $d/a = 2{\cdot}0$.

the spheroid number j as was done in §4 for chains of spheres (see figure 4). The boundary conditions were satisfied at only one point on each object indicating a probable maximum error of 0·6 % based on the two spheroid results.

The solid curves have been drawn to show the change in drag between spheroids within one chain. Comparing these curves with the equivalent drag results for spheres in figure 4, it can be seen that for the case of prolate spheroids less shielding exists within any single chain than in an equivalent chain of spheres. The broken curves in figure 10 demonstrate the change in drag on the jth spheroid in a chain as more spheroids are added to the chain. These curves are

of greater slope than those for spheres (figure 4) once again indicating the weaker shielding characteristics exhibited by a chain of prolate spheroids. As the results in figure 10 were all obtained for spheroids having a spacing parameter (d/a) of 2 the drag on each spheroid in a seven spheroid chain is plotted in figure 11 for different particle spacings. Comparing these results with the

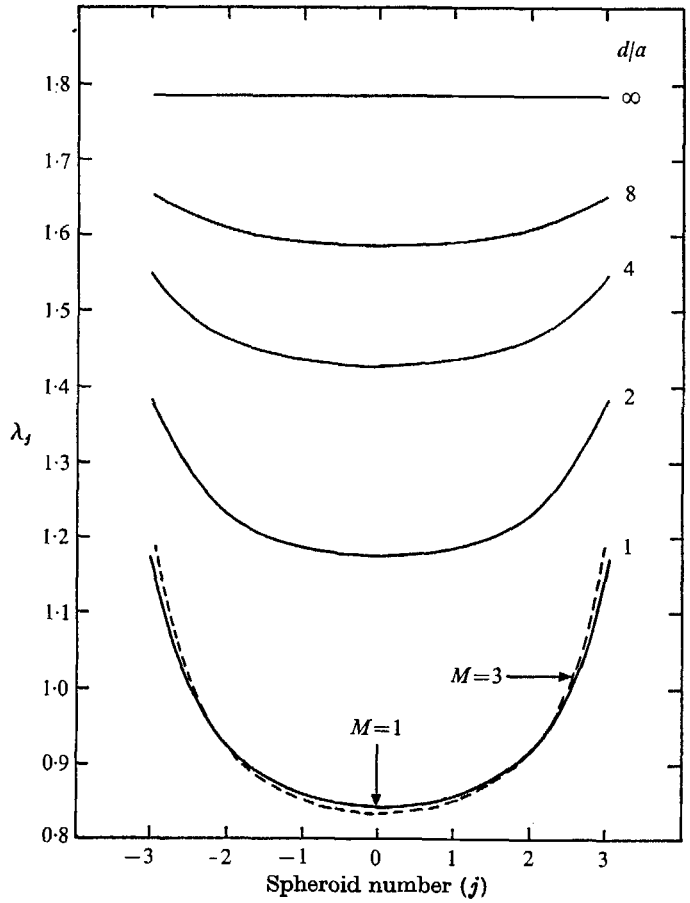

FIGURE 11. Drag correction factor for a chain containing seven prolate spheroids at different spheroid spacings with $a/b = 5{\cdot}0$.

equivalent results for spheres in figure 5 one again observes the weaker shielding effects of prolate spheroids. This comparison also indicates that the interactions between prolate spheroids in a chain will approach zero at smaller values of the spacing parameter than can be expected in the case of spheres.

7. Solutions for multiple oblate spheroids

All the precautionary measures discussed in § 6 to be adopted when applying (5.7) to the case of prolate spheroids apply when (5.7) is used to solve flow problems past oblate spheroids. In addition, it must be kept in mind that for oblate

spheroids the co-ordinate axis p_j is purely imaginary and therefore the Gegenbauer and Legendre functions of the second kind need to be determined using double precision complex arithmetic.

Results for flow past a single oblate spheroid were obtained from (5.7) by considering two oblate spheroids having a spacing parameter (d/a) of 10 000. The boundary conditions were satisfied at the uppermost point on each generating

Aspect ratio, a/b	Spacing parameter, d/a	λ, equation (5.7)	λ, exact Happel & Brenner
0·99	10 000	0·9980	0·9980
0·90	10 000	0·9801	0·9801
0·70	10 000	0·9415	0·9415
0·50	10 000	0·9053	0·9053
0·20	10 000	0·8615	0·8615
0·10	10 000	0·8525	0·8525
0·01	10 000	0·8489	0·8489

TABLE 6. Comparison of drag results for one oblate spheroid from (5.7) with exact solutions of Happel & Brenner (1965)

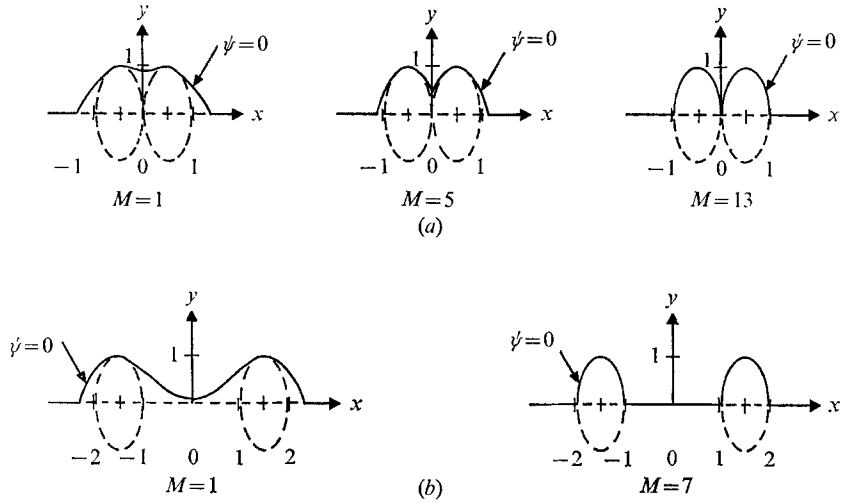

FIGURE 12. Zero streamlines as a function of spheroid spacing and number of boundary points M for oblate spheroids. $a/b = 0{\cdot}5$, (*a*) $d/a = 1$, (*b*) $d/a = 3$.

arc and the results were compared with the exact solutions of Happel & Brenner (1965) in table 6. These results demonstrate that truncated solutions based on the lowest order multipoles agree to four significant digits with the exact solution for the limiting case of flow past a single oblate spheroid for all values of $0{\cdot}01 < a/b < 1{\cdot}0$.

Results showing the convergence of the solution for flow past two oblate spheroids at various spacings where the boundary conditions were satisfied at increasing numbers of points along the generating arc of each spheroid are presented in table 7. Streamlines have been plotted in figure 12 for some cases of interest. The locations of points along the generating arc where the boundary

conditions are to be satisfied are determined by dividing the angle η into equal parts as was done for the case of prolate spheroids. Also from symmetry $\lambda_1 = \lambda_2 = \lambda$.

Table 7 indicates that as for the equivalent cases of flow past spheres and

Aspect ratio, a/b	Spacing, d/a	Number of points, M	λ
0·2	1	1	0·4829
0·2	1	3	0·4672
0·2	1	5	0·4699
0·2	1	7	0·4696
0·2	1	9	0·4697
0·2	1	11	0·4697
0·2	2	1	0·5146
0·2	2	3	0·5007
0·2	2	5	0·5015
0·2	2	7	0·5015
0·2	3	1	0·5410
0·2	3	3	0·5293
0·2	3	5	0·5295
0·2	3	7	0·5295
0·2	4	1	0·5644
0·2	4	3	0·5548
0·2	4	5	0·5548
0·2	8	1	0·6394
0·2	8	3	0·6351
0·2	8	5	0·6351
0·2	16	1	0·7217
0·2	16	3	0·7207
0·2	16	5	0·7207
0·5	1	1	0·5516
0·5	1	3	0·5358
0·5	1	5	0·5374
0·5	1	7	0·5375
0·5	1	9	0·5375
0·5	2	1	0·6103
0·5	2	3	0·6001
0·5	2	5	0·6001
0·5	3	1	0·6571
0·5	3	3	0·6504
0·5	3	5	0·6504
0·5	4	1	0·6939
0·5	4	3	0·6897
0·5	4	5	0·6897
0·5	8	1	0·7771
0·5	8	3	0·7762
0·5	8	5	0·7762
0·5	16	1	0·8349
0·5	16	3	0·8348
0·5	16	5	0·8348

TABLE 7. Convergence results for flow past two oblate spheroids

prolate spheroids convergence to five significant figures is rapidly attained with two oblate spheroids – even when they are touching – as the number of multipoles is increased. It can be seen that convergence to five significant figures is achieved when the boundary conditions are satisfied at only five points on the generating arc of each spheroid, except for the case of two touching spheroids where nine points on each generating arc are required for convergence to four significant figures. By comparing the error in λ shown in table 7 with

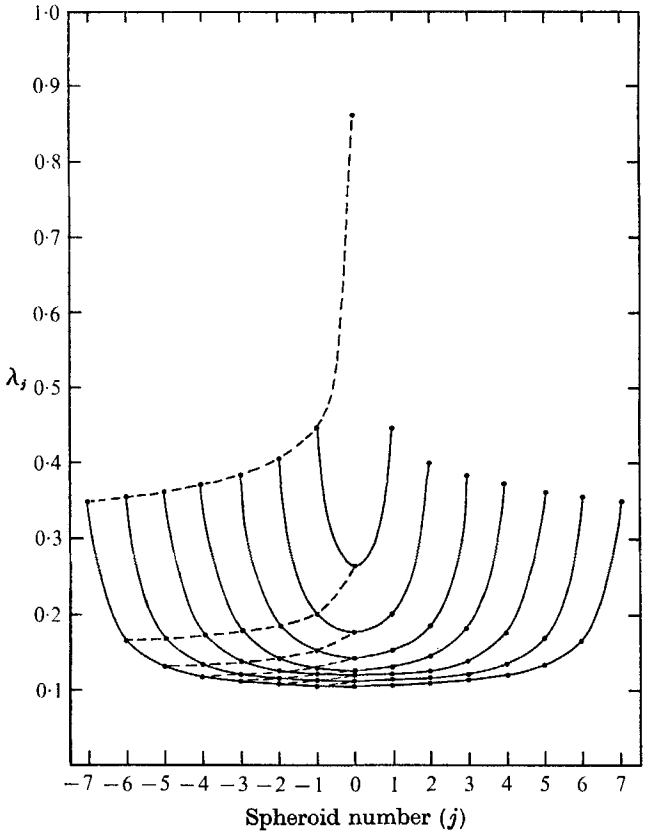

FIGURE 13. Drag correction factor λ_j for chains containing different numbers of oblate spheroids with $a/b = 0{\cdot}2$, $d/a = 2{\cdot}0$.

the equivalent data for spheres and prolate spheroids it can be seen that these errors are approximately equal for touching objects in all three cases. However, as the object spacing increases, errors in λ decrease most rapidly for prolate spheroids and least rapidly for oblate spheroids. Distortions of the zero streamline for two touching oblate spheroids ($a/b = 0{\cdot}5$) and for two spheroids having a d/a ratio of three (figure 12) are greater than the equivalent distortions observed for either spheres or prolate spheroids (figures 3 and 9 respectively). This result is in agreement with the previous observation that streamline distortions are greater for spheres than for prolate spheroids when the boundary conditions are satisfied at only one point on the generating arc of each object, i.e. as the

aspect ratio decreases, the objects become extended in a direction normal to the flow thereby requiring more terms in the series (or higher order multipoles) to describe their boundaries accurately.

Drag results for flow past chains consisting of from one to fifteen oblate spheroids have been plotted in figure 13. These spheroids all have an aspect ratio of 0·2 and a spacing parameter (d/a) of two. As was done for chains of spheres (figure 4) and chains of prolate spheroids (figure 10) the drag correction

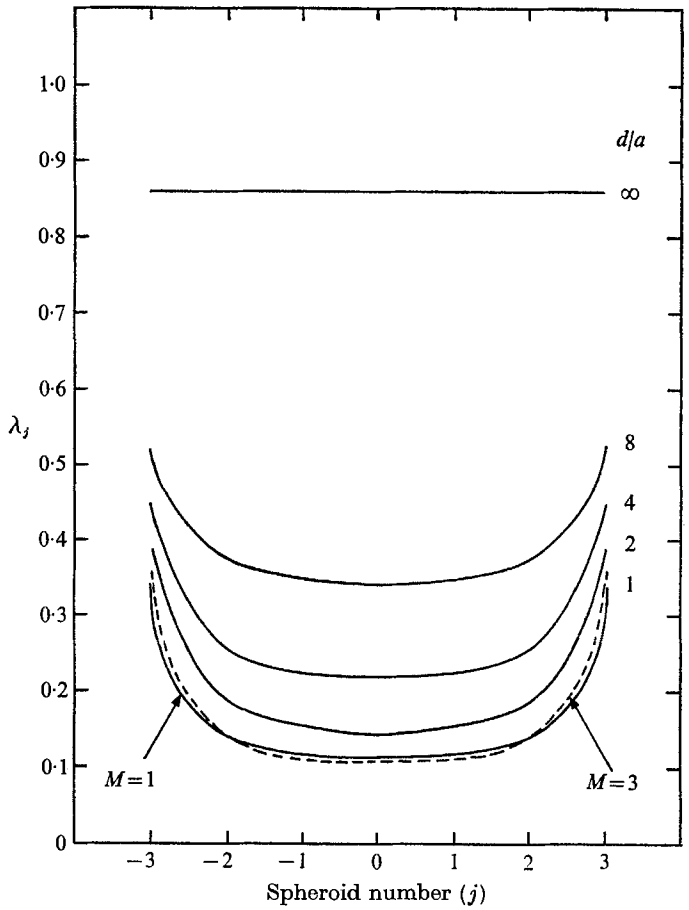

FIGURE 14. Drag correction factor for a chain containing seven oblate spheroids at different spheroid spacings with $a/b = 0{\cdot}2$.

factor λ_j for each oblate spheroid has been plotted against the spheroid number j in figure 13. The boundary conditions were satisfied at only the uppermost point on each spheroid. The percentage error to be expected can be deduced from table 7.

The solid curves showing the change in drag between spheroids in any chain indicate a much stronger shielding effect in a chain of oblate spheroids than was observed for the cases of prolate spheroids or spheres. This assertion is implemented by the almost horizontal nature of the broken curves representing the

change in drag on the jth spheroid in a chain as more spheroids are added to the chain. The results presented in figure 13 were all obtained for spheroids having a spacing parameter (d/a) of two and therefore the drag on each spheroid in a seven spheroid chain is plotted in figure 14 for different particle spacings. Comparing these results with the equivalent results for prolate spheroids (figure 11) and spheres (figure 5) indicates the stronger shielding effects of oblate spheroids. It can also be seen from the relatively slow approach of the λ_j curves to the value for a single oblate spheroid that the interactions between oblate spheroids in a chain will approach zero at larger values of the spacing parameter than can be expected in either the case of chains of prolate spheroids or chains of spheres.

8. Conclusions

This paper is the first in a series of investigations whose overall objective is the development of a new technique for treating the slow viscous motion past finite assemblages of particles of arbitrary shape. The basic idea is that any object in a single or multiple flow configuration can be represented by discrete or continuous distributions of multi-lobular disturbances and approximate representations obtained by truncating these distributions. To illustrate the essential elements of the theory and to show the convergence of the solution procedure the present paper has been confined to a class of simple axially symmetric slow motions for the flow past finite line arrays of spheres or prolate or oblate spheroids. For these flows the boundaries for each object conform to a special natural co-ordinate system. The truncated series of multi-lobular disturbances representing each object have a common origin at the geometric centre of the object. The results indicate, at least for this simple class of flows, that the solution procedure converges more rapidly and is simpler to apply than the method of reflexions, since the solution technique is a single-step truncated matrix inversion rather than a series solution generated through an iterative process. Also, in contrast to the point-force approximation technique, solutions can be obtained to any desired degree of accuracy for all cases even when the objects are touching one another.

Perhaps the most important advantage of the technique for future application is the relatively short amount of computer time required to obtain both flow field solutions and drag results. Some feeling for the rapidity of the calculation technique is gleaned from the fact that the 101 sphere problem described in figure 6 required about 10 sec on an IBM 360–65, which is only a medium capacity present generation computer. This is several orders of magnitude faster than existing finite-difference techniques can handle the flow past only three closely spaced spheres. Also the number of grid points required to treat the finite-difference boundary-value problem for significantly larger numbers of objects would be prohibitive.

The rapidity of the computational technique makes feasible the solution of two classes of problems for which no current satisfactory semi-analytic method exists, (*a*) the slow flow past complex non-slender boundary shapes and (*b*) the

non-steady motion past small finite assemblages of closely spaced objects. In regard to (*a*) the multipole truncation technique is currently being generalized to treat complex axisymmetric objects, such as finite cylinders and cones, that do not possess simple natural co-ordinate systems. The multipole disturbances representing each object in this case do not have a common origin but are distributed along the axis of symmetry. In general, the arbitrary body of revolution can be constructed from a continuous distribution of spheroidal co-ordinate singularities corresponding to touching oblate spheroids of vanishing aspect ratio. The method for obtaining approximate solutions for an arbitrary body of revolution to any desired degree of accuracy using the multipole truncation technique is described in a second forthcoming paper, Gluckman, Pfeffer & Weinbaum (1971*a*). In regard to (*b*) the technique has been applied to the simple unsteady problem of three spheres of arbitrary spacing falling along their line of centres in a gravitational field, Gluckman, Pfeffer & Weinbaum (1971*b*). Finally, it is hoped that the extension of this work to asymmetric flows will result in a useful technique for modelling more varied three-dimensional creeping motion problems relative to finite assemblages of particles of arbitrary shape.

M. J. Gluckman wishes to acknowledge the support and encouragement provided by the St Regis Paper Company for the above work which has been performed as partial fulfillment of the requirements for the Ph.D. degree from the School of Engineering of The City University of New York. The authors also wish to thank the National Science Foundation for supporting this research under Grant no. GK-16506.

REFERENCES

Broersma, S. 1960 *J. Chem. Phys.* **32**, 1632.

Burgers, J. M. 1938 *Second Report on Viscosity and Plasticity.* Amsterdam: North Holland Publishing Co.

Burgers, J. M. 1940 *Proc. Konigl. Akad. Wetenschap. (Amsterdam)*, **43**, 425, 646.

Burgers, J. M. 1941 *Proc. Konigl. Wetenschap. (Amsterdam)*, **44**, 1045.

Burgers, J. M. 1942 *Proc. Konigl. Akad. Wetenschap. (Amsterdam)*, **45**, 9.

Chen, T. C. & Skalak, R. 1970 *Appl. Sci. Res.* **22**, 403.

Davis, M. H. 1969 *Chem. Engng. Sci.* **24**, 1769.

Dean, W. R. & O'Neill, M. E. 1963 *Mathematika*, **10**, 13.

Faxen, H. (with appendix by Dahl) 1925 *Ark. Mat. Astr. Fys.* **19**A, no. 13.

Faxen, H. 1927 *Z. angew. Math. Mech.* **7**, 79.

Gluckman, M. J., Weinbaum, S. & Pfeffer, R. 1971*a* A new technique for treating slow viscous flows: axisymmetric flow past arbitrary bodies of revolution. To be published.

Gluckman, M. J., Pfeffer, R. & Weinbaum, S. 1971*b* A theoretical analysis of three spheres falling along their line of centres in an infinite viscous fluid. To be published.

Goldman, A. J., Cox, R. G. & Brenner, H. 1966 *Chem. Engng. Sci.* **21**, 1151.

Haberman, W. L. & Sayre, R. M. 1958 *David W. Taylor model basin Rep.* no. 1143, Washington, D.C.

Happel, J. & Brenner, H. 1965 *Low Reynolds Number Hydrodynamics.* Prentice-Hall.

Kynch, G. J. 1959 *J. Fluid Mech.* **5**, 193.

McNown, J. S. & Lin, P. N. 1952 *Proc. Second Midwestern Conf. Fluid Mech.* Iowa State University. Reprint in Eng. 109.

O'Brien, V. 1968 *A.I.Ch.E. J.* **14** (6), 870.

Payne, L. E. & Pell, W. H. 1960 *J. Fluid Mech.* **7**, 529.

Sampson, R. A. 1891 *Phil. Trans. Roy. Soc.* A **182**, 449.

Savic, P. 1953 *Nat. Res. Counc. Canada Rep.* no. MT-22.

Slack, G. W. & Matthews, H. W. 1961 *Porton Tech. Paper*, Chemical Defence Exptl. Establishment, Porton, no. 797.

Smoluchowski, M. 1911 *Bull Int. Acad. Polonaise Sci. Lett.* **1A**, 28.

Smoluchowski, M. 1912 *Proc. Fifth Int. Cong. Math.* **2**, 192.

Stimson, M. & Jeffery, O. B. 1926 *Proc. Roy. Soc.* A **111**, 110.

Tam, C. K. W. 1969 *J. Fluid Mech.* **38**, 537.

Tchen, C. 1954 *J. Appl. Phys.* **25**, 463.

Wakiya, S. 1965 *J. Phys. Soc. Japan*, **20** (8), 1502.

Wang, H. & Skalak, R. 1969 *J. Fluid Mech.* **38**, 75.